

¹ A modified and efficient phase field model for the biological transport
² network

³ Qing Xia^a, Xiaoyu Jiang^a, Yibao Li^{a,*}

⁴ *^aSchool of Mathematics and Statistics, Xi'an Jiaotong University, Xi'an 710049, China*

⁵ **Abstract**

This paper aims to establish the biological transport network based on the phase field model. In order to ensure that the topological shape is formed under the guidance of electrical conductivity, we generate the biological networks with sufficient information based on the distributions of the venation of the leaf represented by the reaction-diffusion model. We modify the original energy of the network generating model by considering the auxin gradient property. By applying the gradient flow method to minimize the modified energy, we derive the Poisson type equation for pressure, the reaction-diffusion type equation for the network conductance, and the Allen-Cahn type equation for the phase field. The proposed model is significant on the investigation of phase transitions by considering the gradient properties on the boundaries. We have innovatively added conductivity and phase-field coupling terms that inhibit perpendicular transport of nutrients, making it easy to generate thin branches from the trunk through this model. In order to obtain the second-order temporal accuracy, we take the Crank–Nicolson method for the governing system. To obtain the second-order spatial accuracy, we discretize the coupling system with the central finite difference method and linearize the nonlinear terms semi-explicitly to form a linear system at each time step. The discrete energy dissipation is provably preserved and we can use a larger time step. We apply the preconditioned conjugate gradient method with the multigrid method as a preconditioner to implement a practical algorithm with only linear algebraic complexity. The proposed algorithm is easy to implement and achieves a fast convergence. Various numerical tests are demonstrated to verify the efficiency, stability, and robustness of the proposed method.

⁶ *Keywords:* Energy-dissipation-rate preserving, Biological transport networks, Gradient flow, Adaption,

⁷ Unconditional energy stability

*Corresponding author

Email address: yibaoli@xjtu.edu.cn (Yibao Li)

URL: <http://gr.xjtu.edu.cn/web/yibaoli> (Yibao Li)

8 1. Introduction

9 Efficient and robust networks are the cornerstone of the industrial system for transporting the medium
10 like energy[1], consumables[2], signal[3], nutrients[4], and fluids[5], which make significant sense for interaction
11 of large scale system between multiple missions[6]. For organisms relying on multicellular scales system,
12 the biological transport networks are essential for the connection of different organs or tissues, which is embodied
13 in the vascular networks to transport blood flow with energy and nutrients and remove the metabolites
14 through the branched network[7]. The separation into xylem and phloem provides the similar function for
15 the leaf venation in plants[8]. Fast-growing attention on the development, function and adaptation of the
16 biologic transportation networks verified the significance for the natural community[9, 10]. The complicated
17 biological systems have treelike hierarchical structures[11], e.g., the aorta splits into increasingly smaller and
18 smaller arteries all the way to capillaries, which can be recognized as the minimization of dissipation of the
19 blood flow through the system[12, 13]. Loop-redundant treelike structures can be understood conversely as
20 robustness against damage or fluctuating needs [14, 15].

The biological transport networks are traditionally studied in the optimization framework, in which the energy consumption of the network is minimized under the constraint that the total material cost is constant[15]. However, the structures of networks in living organisms are subject to continuous adaptation, responding to various external and internal stimuli[16]. For instance, blood vessel systems are continuously adapting their structures to meet the changing metabolic demand of the tissue throughout the life of humans and animals[17], which can be observed specifically in experiments that blood vessels can sense the wall shear stress to adapt their diameters correspondingly[18, 19]. Mathematical modeling of transportation networks is initially based on discrete frameworks, in particular mathematical graph theory and discrete energy optimization[20, 21]. Cai and Hu[12] proposed a discrete model which can be reformulated into a system of ordinary differential equations to study network dynamics. In their work, a global energy functional approach is suggested considering both material and metabolism costs, nevertheless the corresponding gradient flow ends up driven by the wall shear stress on the tube walls. Several studies appeared under the discrete framework[18, 22, 23], which responded only to local information and incorporated fluctuations in flow. However, these attempts were difficult to explain how angiogenesis and adaptation lead to stable and efficient capillaries[24], particularly, no clear global designing principle of such networks was present to guarantee their efficiency and robustness[25]. Considering that the large-scale structure of transport networks results from adaptive construction corresponding to continuous local requirements, Hu and Cai [26] proposed an optimization principle to drive the formation of biological transport networks underlies potential and common mechanisms. They considered the competition between the reduction of material and metabolic consumptions and the reduction of transport energy cost, which was proved theoretically and numerically to play a dominant role for the induction of the biological network. Then the generalized

continuum model was composed of a spatial-temporal PDE system for a vector conductance variable and an elliptic equation constraint in space for a pressure-like variable[27, 28].

$$-\nabla \cdot ((r(\mathbf{x})\mathbf{I} + \mathbf{m} \otimes \mathbf{m}) \nabla p) = S, \quad (1a)$$

$$\frac{\partial \mathbf{m}}{\partial t} - K\Delta \mathbf{m} - C(\mathbf{m} \cdot \nabla p) \nabla p + \alpha |\mathbf{m}|^{2(\gamma-1)} \mathbf{m} = 0. \quad (1b)$$

We denote the conductance vector as $\mathbf{m}(t, \mathbf{x}) \in \Omega$, where the tissue domain Ω is a bounded domain with a smooth boundary $\partial\Omega$. The direction of \mathbf{m} stands for the direction of active transport and the amplitude $|\mathbf{m}|$ quantifies the transport strength. Let us denote $p(\mathbf{x}, t)$ as the pressure of the relevant hormone, $r(\mathbf{x})$ as the background permeability, I as the identity matrix, $S(\mathbf{x})$ as the distribution of the hormone source produced in the tissue, $K \geq 0$ as the diffusivity parameter, $C \geq 0$ as the activation parameter driving the network adaptation, $\alpha \geq 0$ as the metabolic constant, and $\gamma \in [1/2, 1]$ as the metabolic rate of the bio-organism according to Murray's Law[29], respectively. Let us consider the original energy cost functional \mathcal{E}_M as

$$\mathcal{E}_M = \frac{1}{2} \int_{\Omega} \left(K|\nabla \mathbf{m}|^2 + \frac{\alpha}{\gamma} |\mathbf{m}|^{2\gamma} + C|\mathbf{m} \cdot \nabla p|^2 + Cr|\nabla p|^2 \right) d\mathbf{x}, \quad (2)$$

where the first term $K|\nabla \mathbf{m}|^2$ is the entropy cost responsible for active transport. The second term $\alpha|\mathbf{m}|^{2\gamma}/\gamma$ shows the material and metabolic energy cost of maintaining the active transport or constructing the transport network edges. The last term $(C|\mathbf{m} \cdot \nabla p|^2 + Cr|\nabla p|^2)$ is the average energy cost for all different states with fluctuating fluxes. This model drives the canalisation by coupling the hormone transport and the adaptation process.

Following the continuum models, two paths were carried out for the development of biological transport networks[6]: one emphasized optimization of energy cost and established the theoretical framework on the existence of analytical solutions. The other focused on generating the numerical adaptation mechanism by coupling the relevant stimuli and developing the corresponding network generating schemes. Haskovec et al. [30] proved the existence of global weak solutions and local mild solutions. They used a geometric perturbation argument to prove the existence of nontrivial steady states, which implied that long term convergence of the transient solutions towards steady states. Furthermore, they extended the results obtained previously to the whole range of meaningful relaxation exponents by regarding the existence of weak and mild solutions[31]. Li[32] established the local existence of strong solutions and presented a blow-up criterion, whose global existence were rigorously proved under some smallness conditions of the initial data and the source. By applying the Dirichlet heat semigroup and the properties of divergence equations, the authors [33] established the existence of the steady states by means of dynamical methods and proved that Dirichlet-Neumann initial-boundary possesses a globally classical solution which is unique and uniformly bounded. Ronellenfitsch et al.[34] explored analytically and numerically the design, efficiency and topology of noise-

canceling networks, and provided concrete guiding principles for designing more robust and efficient power grids and sensor networks. The analytical solutions can be used to demonstrate the physical significance and provided the opportunity for the exploration at complicated cases without analytical solution. Due to the rigidity and high nonlinearity of the biological generating system, it is difficult to find the closed form solution and provide the corresponding theoretical analysis under the corresponding initial values and bounds. The researchers gradually focused on the exploration of numerical solutions to establish the efficient and stable numerical schemes. Fang et al.[35] developed the implicit and semi-implicit time discretizations for the Cai-Hu model to overcome the numerical challenges including the nonlinearity and stiffness. Their proposed scheme was energy stable, which were proved in one dimension and verified numerically in two dimension. Haskovec et al. [31] applied the variational formulation based on the penalty method to construct the stationary solutions for the case of vanishing diffusion and critical value of the relaxation exponent. They used the numerical method to prove the analytical results adopted to the one dimensional setting can be valid in several space dimensions. Hong et al. [36, 37] recast the network generating partial differential equation system into the singular limit of a dissipative gradient flow model and developed several structure-preserving numerical algorithms for the gradient flow model based on the energy quadratization method. Their numerical scheme preserved the dissipation rate in the discrete sense with second-order accurate, efficient, linear properties. Facca et al. [38] presented an extension of the Cai-Hu model that considers the time derivative of the conductivity, which grows as a power-law of the transport flux. Hu et al. [39] were inspired by the Cai-Hu model to construct the formulation of flow networks where the fluid is modeled by the Darcy-Stokes flow with the presence of volume sources. They adopted filtering techniques to design suitable objective functionals to console the challenges caused by the non-convex optimization property and ill-posedness.

In this paper, we aim to establish the biological transport network based on the phase field model. The phase field model has been shown to be adaptable in various fields, such as topology optimization[40, 41], additive manufacturing[42, 43], multi-component fluid flows[44, 45], and image processing[46, 47]. We will introduce the internal chemical potential energy, which naturally concentrates the auxin gradient property and determinate the generation of the biological network, to modify the original energy of Cai-Hu model. Then the complicated model, which couples the Poisson type equation for pressure, the reaction-diffusion type equation for the network conductance, and the Allen-Cahn type equation for phase field, will be derived as a gradient flow by minimizing the modified energy consumed by the system. The rigorous proof of the energy dissipation will be confirmed in detail. The governing system is discretized by the Crank–Nicolson method to maintain the second-order temporal accuracy. The spatial discretization of the coupling equations is achieved under the finite difference framework. We prove that the discrete energy dissipation is preserved unconditionally, which confirms that a larger time step can be used. In order to implement a practical algorithm with only linear algebraic complexity and achieve fast convergence, we

82 apply the preconditioned conjugate gradient method with the multigrid method as a preconditioner. The
83 biological network model is decoupled and the proposed algorithm is easy to implement. Comparing to the
84 existing models on the investigation of biological transport network, the advantages of our phase field based
85 method are summarized as follows: (i) We modified the biological network generating model to consider
86 the auxin gradient properties, which plays significant role in suppressing the transport perpendicular to
87 the phase boundaries and forming the branches from the trunk. The proposed model is proved to satisfy
88 the energy dissipation, which corresponds to the physical context. (ii) Our numerical solutions are efficient
89 and stable, which can achieve second-order accuracy in space and time. To solve the resulting system of
90 discrete equations, we will use the multigrid preconditioned conjugate gradient method, which has $O(N)$
91 computational complexity. The proposed method has inherent high parallelism and improves convergence
92 of long wavelength components. (iii) Our discrete method is simple and easy to implement since it is
93 completely decoupled and has linear algebraic computational complexity. The discrete system is proved
94 to be unconditionally energy stable and so that we can use a larger time step. Several representative
95 computational tests are demonstrated to validate the efficiency, stability and applicability of the proposed
96 scheme.

97 The rest of the paper is organized as follows. We review the general gradient flow system. Then we modify
98 the total energy and transform the original governing equations into the phase field framework in Section
99 2. We describe the discrete scheme with second-order temporal accuracy based on a Crank–Nicolson-type
100 method and rigorously prove the discrete energy dissipation in Section 3. Various numerical experiments are
101 carried out by using benchmark examples in Section 4. Finally, a concluding remark is presented in Section
102 5.

103 2. Methodology

104 In this section, we apply the variational formulation to generate the biological network PDE model.
105 Based on the generalized Onsager principle [48], the gradient flow model is proposed with the nonlin-
106 ear, time-independent equation. By adopting a specific chemical potential energy, i.e., Ginzburg–Landau
107 energy[49], into the original energy function, we modify the original governing equation as the energy-
108 dissipative biological-network-generating PDE model based on the phase field method. Then the investiga-
109 tion on the well-posedness and energy dissipation of the gradient flow model are validated with modified
110 network-generating model. The relevant and compatible boundary conditions have been discussed to fit the
111 corresponding physical model.

¹¹² 2.1. Review of the gradient flow model

By introducing an artificial time variable t , we aim to find a stationary order parameter \mathbf{m} in the following gradient flow:

$$\frac{\partial \mathbf{m}}{\partial t} = -\frac{\delta \mathcal{E}_M}{\delta \mathbf{m}}. \quad (3)$$

The derivation of the conductance vector \mathbf{m} in a gradient flow is reviewed as:

$$\begin{aligned} \left(\frac{\delta \mathcal{E}_M}{\delta \mathbf{m}}, \mathbf{g} \right)_{L_2} &= \frac{d}{d\eta} \mathcal{E}_M(p, \mathbf{m} + \eta \mathbf{g}) \Big|_{\eta=0} \\ &= \int_{\Omega} \left(-K \Delta \mathbf{m} + \alpha |\mathbf{m}|^{2(\gamma-1)} \mathbf{m} - C(\mathbf{m} \cdot \nabla p) \nabla p \right) \cdot \mathbf{g} d\mathbf{x}. \end{aligned}$$

The stationary order parameter p can be obtained in the following gradient flow:

$$S = \frac{\delta \mathcal{E}_M}{\delta p}, \text{ with } \int_{\Omega} S d\mathbf{x} = 0, \quad (4)$$

where the chemical potential $\delta \mathcal{E}/\delta p$ can be obtained via the variational derivative of the objective functional Eq. (2) with respect to p as

$$\left(\frac{\delta \mathcal{E}_M}{\delta p}, q \right)_{L_2} = \frac{d}{d\eta} \mathcal{E}_M(p + \eta q, \mathbf{m}) \Big|_{\eta=0} = \int_{\Omega} \left(-C \nabla \cdot (r \mathbf{I} + \mathbf{m} \otimes \mathbf{m}) \nabla p \right) q d\mathbf{x}.$$

Here p is the partial pressure of the relevant hormone and satisfies the Kirchoff's laws for obtaining the flow distribution in the vascular network. We should remark that since the time scale of fluctuations is not comparable to that of the transport, we use the steady-state transport equation to avoid the reduction in the strength of fluctuations in flux. Then we derive the following governing equations

$$\begin{cases} -\nabla \cdot ((r(\mathbf{x}) \mathbf{I} + \mathbf{m} \otimes \mathbf{m}) \nabla p) = S, \\ \frac{\partial \mathbf{m}}{\partial t} = K \Delta \mathbf{m} + C (\mathbf{m} \cdot \nabla p) \nabla p - \alpha |\mathbf{m}|^{2(\gamma-1)} \mathbf{m}, \end{cases} \quad (5)$$

¹¹³ where \otimes is the tensor product. Thus we can obtain the following energy dissipation law:

Theorem 1. The governing system Eq. (5) preserves the energy dissipation as follows:

$$\frac{\partial \mathcal{E}_M}{\partial t} = \int_{\Omega} -|\mathbf{m}_t|^2 d\mathbf{x} \leq 0. \quad (6)$$

Proof. By taking the derivative formulation of the original energy Eq. (2) with respect to time and substituting equations Eqs. (5) into the derivation functional, the energy dissipation can be obtained as

follows:

$$\begin{aligned}
\frac{\partial \mathcal{E}_M}{\partial t} &= \int_{\Omega} K \nabla \mathbf{m} \cdot \nabla \mathbf{m}_t + \alpha |\mathbf{m}|^{2\gamma-1} \cdot \frac{\mathbf{m}}{|\mathbf{m}|} \mathbf{m}_t d\mathbf{x} \\
&\quad + \int_{\Omega} C(\mathbf{m} \cdot \nabla p) \cdot (\mathbf{m}_t \cdot \nabla p + \mathbf{m} \cdot \nabla p_t) + Cr \nabla p \cdot \nabla p_t d\mathbf{x} \\
&= \int_{\Omega} -K \Delta \mathbf{m} \cdot \mathbf{m}_t + \alpha |\mathbf{m}|^{2(\gamma-1)} \mathbf{m} \cdot \mathbf{m}_t - C(\mathbf{m} \cdot \nabla p) \nabla p \cdot \mathbf{m}_t \\
&\quad + C(\mathbf{m} \otimes \mathbf{m}) \nabla p \cdot \nabla p_t + Cr \nabla p \cdot \nabla p_t d\mathbf{x} + \int_{\partial\Omega} K \mathbf{n} \mathbf{m} : \nabla \mathbf{m}_t ds \\
&= \int_{\Omega} -\mathbf{m}_t \cdot \mathbf{m}_t d\mathbf{x} + \int_{\partial\Omega} K \mathbf{n} \mathbf{m} : \nabla \mathbf{m}_t ds - C \int_{\Omega} \nabla \cdot ((r\mathbf{I} + \mathbf{m} \otimes \mathbf{m}) \nabla p) p_t d\mathbf{x} \\
&\quad + \int_{\partial\Omega} C \mathbf{n} \cdot (r\mathbf{I} + \mathbf{m} \otimes \mathbf{m}) \cdot \nabla p p_t ds \\
&= \int_{\Omega} -\mathbf{m}_t \cdot \mathbf{m}_t d\mathbf{x} + \int_{\partial\Omega} K \mathbf{n} \mathbf{m} : \nabla \mathbf{m}_t + C \mathbf{n} \cdot (r\mathbf{I} + \mathbf{m} \otimes \mathbf{m}) \cdot \nabla p p_t ds \\
&= \int_{\Omega} -|\mathbf{m}_t|^2 d\mathbf{x} \leq 0.
\end{aligned}$$

Here the following boundary conditions have been applied as

$$\mathbf{n} \cdot \nabla \mathbf{m}_t = 0, \text{ and } \mathbf{n} \cdot (r\mathbf{I} + \mathbf{m} \otimes \mathbf{m}) \cdot \nabla p = 0, \quad (7)$$

¹¹⁴ which implies additional consistency condition $\int_{\Omega} S d\mathbf{x} = 0$ has been used to keep the isolated property. The
¹¹⁵ proof is completed. \square

¹¹⁶ 2.2. Phase field model coupled with the biological transport network

¹¹⁷ In this section, the phase field model for generating the biological transport network is considered.
¹¹⁸ According to the mathematical analysis on the distributions of the venation of the leaf[50], the reaction
¹¹⁹ diffusion model, which naturally concentrates the auxin gradient property, provides the biological networks
¹²⁰ with sufficient information to determine their generation. The temporal changes of the auxin concentration
¹²¹ inside a region depends on the difference between diffusion and production. Let us begin with the Ginzburg-
¹²² Landau energy

$$\mathcal{E}_{\phi} = \int_{\Omega} (F(\phi)/\epsilon^2 + |\nabla \phi|^2/2) d\mathbf{x}, \quad (8)$$

¹²³ where $F(\phi) = 0.25\phi^2(1-\phi)^2$, and $\epsilon > 0$ is the interfacial thickness of vessel wall. The designed variable ϕ
¹²⁴ is allowed to have values in $[0, 1]$ instead of only 0 or 1. Let us replace the hyper surface between the leaf
¹²⁵ venation and nutrient by the interfacial layer with thickness proportional to the small parameter ϵ . In order
¹²⁶ to ensure that the topological shape formed by the flow of nutrient can be characterized under the guidance
¹²⁷ of electrical conductivity, we add the convective term $\mathcal{E}_C = \int_{\Omega} |\mathbf{m} \cdot \nabla \phi|^2/2 d\mathbf{x}$ to the energy function. By

¹²⁸ combining the metabolic cost energy with the Ginzburg-Landau energy, we can obtain the modified total
¹²⁹ energy as

$$\begin{aligned}\mathcal{E}_N &= \mathcal{E}_M + \mathcal{E}_\phi + \mathcal{E}_C \\ &= \frac{1}{2} \int_{\Omega} \left(K|\nabla \mathbf{m}|^2 + \frac{\alpha}{\gamma} |\mathbf{m}|^{2\gamma} + C|\mathbf{m} \cdot \nabla p|^2 + Cr|\nabla p|^2 \right) d\mathbf{x} \\ &\quad + \beta \int_{\Omega} \left(F(\phi)/\epsilon^2 + |\nabla \phi|^2/2 \right) d\mathbf{x} + \zeta \int_{\Omega} |\mathbf{m} \cdot \nabla \phi|^2/2 d\mathbf{x},\end{aligned}\tag{9}$$

¹³⁰ where we use β to be the positive penalized parameter and use positive parameter ζ to control the convective
¹³¹ effect on the conductivity. From a constrained gradient flow of the energy cost functional Eq. (9), we can
¹³² derive the Allen-Cahn equation, which has been applied in various applications as the following gradient
¹³³ flow:

$$\frac{\partial \phi}{\partial t} = -\frac{\delta \mathcal{E}_N}{\delta \phi},\tag{10}$$

from which we can obtain the phase field functional via variational derivative of the energy functional with respect to ϕ as

$$\begin{aligned}\left(\frac{\delta \mathcal{E}_N}{\delta \phi}, \psi \right)_{L_2} &= \frac{d}{d\eta} \mathcal{E}_N(p, \mathbf{m}, \phi + \eta\psi) \Big|_{\eta=0} \\ &= \beta \int_{\Omega} \left(\frac{F'(\phi)}{\epsilon^2} - \Delta \phi \right) \psi d\mathbf{x} + \zeta \int_{\Omega} (\mathbf{m} \otimes \mathbf{m}) \nabla \phi \cdot \nabla \psi d\mathbf{x} \\ &= \beta \int_{\Omega} \left(\frac{F'(\phi)}{\epsilon^2} - \Delta \phi \right) \psi d\mathbf{x} - \zeta \int_{\Omega} \nabla \cdot ((\mathbf{m} \otimes \mathbf{m}) \cdot \nabla \phi) \psi d\mathbf{x} + \zeta \int_{\partial\Omega} (\mathbf{n} \cdot (\mathbf{m} \otimes \mathbf{m}) \cdot \nabla \phi) \psi ds \\ &= \int_{\Omega} \left(\beta \left(\frac{F'(\phi)}{\epsilon^2} - \Delta \phi \right) - \zeta \nabla \cdot ((\mathbf{m} \otimes \mathbf{m}) \cdot \nabla \phi) \right) \psi d\mathbf{x},\end{aligned}$$

¹³⁴ where the boundary condition $\mathbf{n} \cdot (\mathbf{m} \otimes \mathbf{m}) \cdot \nabla \phi = 0$ is applied. The gradients of the production, diffusion and
¹³⁵ differentiation shown in tissue-specific regulatory mechanism[51] can be paired with the reaction-diffusion
¹³⁶ equation. The constant parameters of diffusive transport and production are used to coordinate the global
¹³⁷ information with the vein generation. Thus the leaf vein patterning can be obtained by the proposed gradient
¹³⁸ flow model and provides the opportunities for the communication between different parts of the biological
¹³⁹ tissue. The modified parameter \mathbf{m} can be obtained in the following gradient flow

$$\frac{\partial \mathbf{m}}{\partial t} = -\frac{\delta \mathcal{E}_N}{\delta \mathbf{m}},\tag{11}$$

from which we can obtained the vector-value conductance functional via variational derivative of the energy functional with respect to \mathbf{m} as

$$\begin{aligned} \left(\frac{\delta \mathcal{E}_N}{\delta \mathbf{m}}, \mathbf{g} \right)_{L_2} &= \frac{d}{d\eta} \mathcal{E}_N(p, \mathbf{m} + \eta \mathbf{g}, \phi) \Big|_{\eta=0} \\ &= \int_{\Omega} \left(-K\Delta \mathbf{m} + \alpha |\mathbf{m}|^{2(\gamma-1)} \mathbf{m} - C(\mathbf{m} \cdot \nabla p) \nabla p - \zeta(\mathbf{m} \cdot \nabla \phi) \nabla \phi \right) \cdot \mathbf{g} d\mathbf{x}. \end{aligned}$$

Thus, we can modify the original governing system (Eq. (5)) as:

$$\begin{aligned} \frac{\partial \phi}{\partial t}(\mathbf{x}, t) &= -\beta \left(\frac{F'(\phi(\mathbf{x}, t))}{\epsilon^2} - \Delta \phi(\mathbf{x}, t) \right) \\ &\quad + \zeta \nabla \cdot ((\mathbf{m}(\mathbf{x}, t) \otimes \mathbf{m}(\mathbf{x}, t)) \nabla \phi(\mathbf{x}, t)), \end{aligned} \tag{12a}$$

$$-\nabla \cdot ((r(\mathbf{x})\mathbf{I} + \mathbf{m}(\mathbf{x}, t) \otimes \mathbf{m}(\mathbf{x}, t)) \nabla p(\mathbf{x}, t)) = S(\mathbf{x}), \tag{12b}$$

$$\begin{aligned} \frac{\partial \mathbf{m}}{\partial t}(\mathbf{x}, t) &= K\Delta \mathbf{m}(\mathbf{x}, t) + C(\mathbf{m}(\mathbf{x}, t) \cdot \nabla p(\mathbf{x}, t)) \nabla p(\mathbf{x}, t) \\ &\quad - \alpha |\mathbf{m}(\mathbf{x}, t)|^{2(\gamma-1)} \mathbf{m}(\mathbf{x}, t) + \zeta (\mathbf{m}(\mathbf{x}, t) \cdot \nabla \phi(\mathbf{x}, t)) \nabla \phi(\mathbf{x}, t). \end{aligned} \tag{12c}$$

¹⁴⁰ Based on the modified system Eqs. (12), we can obtain the following energy dissipation law:

Theorem 2. The governing equations Eqs. (12) preserve the energy production rate as follows

$$\frac{\partial \mathcal{E}_N}{\partial t} = \int_{\Omega} -|\mathbf{m}_t|^2 d\mathbf{x} + \int_{\Omega} -|\phi_t|^2 d\mathbf{x} \leq 0. \tag{13}$$

Proof. By taking the derivative formulation of the modified energy Eq. (9) with respect to time and substituting equations Eqs. (12) into the derivation functional, the energy dissipation can be obtained as follows:

$$\begin{aligned} \frac{\partial \mathcal{E}_N}{\partial t} &= \int_{\Omega} K \nabla \mathbf{m} \cdot \nabla \mathbf{m}_t + \alpha |\mathbf{m}|^{2\gamma-1} \cdot \frac{\mathbf{m}}{|\mathbf{m}|} \mathbf{m}_t + Cr \nabla p \cdot \nabla p_t \\ &\quad + C(\mathbf{m} \cdot \nabla p) \cdot (\mathbf{m}_t \cdot \nabla p) + C(\mathbf{m} \cdot \nabla p) \cdot (\mathbf{m} \cdot \nabla p_t) d\mathbf{x} \\ &\quad + \int_{\Omega} \zeta (\mathbf{m} \cdot \nabla \phi) \cdot (\mathbf{m}_t \nabla \phi + \mathbf{m} \nabla \phi_t) + \beta \frac{F'(\phi)}{\epsilon^2} \phi_t + \beta \nabla \phi \cdot \nabla \phi_t d\mathbf{x} \\ &= \int_{\Omega} -K \Delta \mathbf{m} \cdot \mathbf{m}_t + \alpha |\mathbf{m}|^{2(\gamma-1)} \mathbf{m} \cdot \mathbf{m}_t - C(\mathbf{m} \cdot \nabla p) \nabla p \cdot \mathbf{m}_t \\ &\quad + C(r\mathbf{I} + \mathbf{m} \otimes \mathbf{m}) \nabla p \cdot \nabla p_t - \zeta (\mathbf{m} \cdot \nabla \phi) \nabla \phi \cdot \mathbf{m}_t d\mathbf{x} \\ &\quad + \zeta \int_{\partial\Omega} K \mathbf{n} \mathbf{m} : \nabla \mathbf{m}_t ds + \int_{\Omega} \zeta (\mathbf{m} \otimes \mathbf{m}) \nabla \phi \cdot \nabla \phi_t d\mathbf{x} + \int_{\Omega} \beta \left(\frac{F'(\phi)}{\epsilon^2} - \Delta \phi \right) \phi_t d\mathbf{x} \\ &= \int_{\Omega} -|\mathbf{m}_t|^2 d\mathbf{x} + \int_{\Omega} \left(\beta \left(\frac{F'(\phi)}{\epsilon^2} - \Delta \phi \right) - \zeta \nabla \cdot ((\mathbf{m} \otimes \mathbf{m}) \nabla \phi) \right) \phi_t d\mathbf{x} \end{aligned}$$

$$\begin{aligned}
& + \int_{\partial\Omega} K \mathbf{n} \mathbf{m} : \nabla \mathbf{m}_t ds + \int_{\partial\Omega} C \mathbf{n} \cdot (rI + \mathbf{m} \otimes \mathbf{m}) \cdot \nabla p p_t ds \\
& + \int_{\partial\Omega} \zeta \mathbf{n} \cdot (\mathbf{m} \otimes \mathbf{m}) \cdot \nabla \phi \phi_t ds \\
= & \int_{\Omega} -|\mathbf{m}_t|^2 d\mathbf{x} + \int_{\Omega} -|\phi_t|^2 d\mathbf{x} \leq 0,
\end{aligned}$$

where the following boundary conditions have been applied as

$$\mathbf{n} \cdot \nabla \mathbf{m}_t = \mathbf{0}, \quad \mathbf{n} \cdot (r\mathbf{I} + \mathbf{m} \otimes \mathbf{m}) \cdot \nabla p = 0, \quad \text{and } \mathbf{n} \cdot (\mathbf{m} \otimes \mathbf{m}) \cdot \nabla \phi = 0. \quad (14)$$

¹⁴¹ Note that the additional consistency condition $\int_{\Omega} S d\mathbf{x} = 0$ should be used to keep the isolated property.
¹⁴² The proof is completed. \square
¹⁴³ We should claim that the energy cost function introduced in Eq. (9) directly suppresses the transport
¹⁴⁴ perpendicular to the phase boundaries. However, the original energy of the network generating model is
¹⁴⁵ modified by considering the auxin gradient property, while it can insignificantly affect the vector field of
¹⁴⁶ \mathbf{m} . Furthermore, the proposed energy cost function can help to stabilize the boundaries between different
¹⁴⁷ phases (venation phase and tissue phase) and improve the stability of numerical schemes, which can be
¹⁴⁸ validated numerically in the below section.

¹⁴⁹ 3. Numerical Solutions

¹⁵⁰ The numerical solution of our proposed biological transport network generating system is performed
¹⁵¹ by using the second-order accurate spatial discretization and the second-order accurate Crank-Nicolson
¹⁵² discretization. Let us first present the numerical method in two dimension, which can be extended to three
¹⁵³ dimension in a straightforward manner without loss of generalities. Let us discretize the bounded domain
¹⁵⁴ $\Omega = [0, L_x] \times [0, L_y] \subset \mathcal{R}^2$ as $\Omega_d = \{(x_i, y_i) : 1 \leq i \leq N_x, 1 \leq i \leq N_y\}$, where N_x and N_y are even integers.
¹⁵⁵ Let \mathbf{m}_{ij}^n be the approximation to $\mathbf{m}(x_i, y_j, n\Delta t)$, where $x_i = (i - 0.5)h, y_j = (j - 0.5)h, \Delta t = T/N_t$ is
¹⁵⁶ the time step with the total computational time T and the number of computational time steps N_t , and
¹⁵⁷ $h = L_x/N_x = L_y/N_y$ is defined as the uniform mesh size. The discrete expressions of $\phi(x_i, y_j, n\Delta t)$ and
¹⁵⁸ $p(x_i, y_j, n\Delta t)$ are in the same manner. The cell vertices are located at $(x_{i+\frac{1}{2}}, y_{j+\frac{1}{2}}) = (ih, jh)$. Let us
¹⁵⁹ define the discrete gradient operator as

$$\nabla_d \phi_{i,j} = \left(D_x \phi_{i+\frac{1}{2},j}, D_y \phi_{i,j+\frac{1}{2}} \right), \quad (15)$$

where $D_x \phi_{i+\frac{1}{2},j} = (\phi_{i+1,j} - \phi_{i,j})/h$ and $D_y \phi_{i,j+\frac{1}{2}} = (\phi_{i,j+1} - \phi_{i,j})/h$. The discrete Laplacian operator can be defined as

$$\Delta_d \phi_{i,j} = (\phi_{i-1,j} + \phi_{i+1,j} + \phi_{i,j-1} + \phi_{i,j+1} - 4\phi_{i,j})/h^2. \quad (16)$$

Furthermore, let us define the discrete inner products and discrete norms as:

$$\begin{aligned} (\phi, \psi)_d &= h^2 \sum_{i=1}^{N_x} \sum_{j=1}^{N_y} \phi_{i,j} \psi_{i,j}, \\ (\nabla_d \phi, \nabla_d \psi)_d &= h^2 \sum_{i=1}^{N_x} \sum_{j=1}^{N_y} \left(D_x \phi_{i+\frac{1}{2},j} D_x \psi_{i+\frac{1}{2},j} + D_y \phi_{i,j+\frac{1}{2}} D_y \psi_{i,j+\frac{1}{2}} \right), \\ \|\phi\|_d^2 &= (\phi, \phi)_d, \quad \|\nabla_d \phi\|_d^2 = (\nabla_d \phi, \nabla_d \phi)_d, \\ \|\nabla_d \mathbf{m}\|_d^2 &= \|D_x m_1\|_d^2 + \|D_y m_1\|_d^2 + \|D_x m_2\|_d^2 + \|D_y m_2\|_d^2. \end{aligned}$$

160 3.1. Second-order accuracy discrete system

In order to achieve the second-order accuracy with respect to time and space, we use the standard central difference discretization scheme and Crank Nicolson scheme to get the governing equations:

$$\nabla_d \cdot \left(\left(r\mathbf{I} + \tilde{\mathbf{m}}^{n+\frac{1}{2}} \otimes \tilde{\mathbf{m}}^{n+\frac{1}{2}} \right) \nabla_d p^{n+\frac{1}{2}} \right) = S, \quad (17a)$$

$$\begin{aligned} \frac{\mathbf{m}^{n+1} - \mathbf{m}^n}{\Delta t} &= K \Delta_d \mathbf{m}^{n+\frac{1}{2}} + C \left(\tilde{\mathbf{m}}^{n+\frac{1}{2}} \cdot \nabla_d p^{n+\frac{1}{2}} \right) \nabla_d p^{n+\frac{1}{2}} \\ &\quad - \alpha \|\tilde{\mathbf{m}}^{n+\frac{1}{2}}\|_d^{2(\gamma-1)} \mathbf{m}^{n+\frac{1}{2}} + \zeta \left(\tilde{\mathbf{m}}^{n+\frac{1}{2}} \cdot \nabla_d \tilde{\phi}^{n+\frac{1}{2}} \right) \nabla_d \tilde{\phi}^{n+\frac{1}{2}}, \end{aligned} \quad (17b)$$

$$\begin{aligned} \frac{\phi^{n+1} - \phi^n}{\Delta t} &= -\frac{\beta}{\epsilon^2} \left(F' \left(\tilde{\phi}^{n+\frac{1}{2}} \right) + \xi \phi^{n+\frac{1}{2}} - \xi \tilde{\phi}^{n+\frac{1}{2}} \right) + \beta \Delta_d \phi^{n+\frac{1}{2}} \\ &\quad + \zeta \nabla_d \cdot \left(\left(\tilde{\mathbf{m}}^{n+\frac{1}{2}} \otimes \tilde{\mathbf{m}}^{n+\frac{1}{2}} \right) \nabla_d \tilde{\phi}^{n+\frac{1}{2}} \right), \end{aligned} \quad (17c)$$

161 where $(\cdot)^{n+\frac{1}{2}} = 0.5(\cdot)^{n+1} + 0.5(\cdot)^n$, $(\cdot)^{\widetilde{n+\frac{1}{2}}} = 1.5(\cdot)^n - 0.5(\cdot)^{n-1}$. The outline of the numerical solution for 162 Eqs. (17) in one time step is as follows:

163 **Step 1.** Initialize \mathbf{m}^0 , \mathbf{m}^{-1} , p^0 , p^{-1} , ϕ^0 , and ϕ^{-1} , respectively.

164 **Step 2.** Solve Eq. (17a) to get p^{n+1} from \mathbf{m}^n , \mathbf{m}^{n-1} , and p^n .

Let us consider $\nabla_d \cdot \left(\left(r\mathbf{I} + \tilde{\mathbf{m}}^{n+\frac{1}{2}} \otimes \tilde{\mathbf{m}}^{n+\frac{1}{2}} \right) \nabla_d p^{n+\frac{1}{2}} \right)$ as

$$\begin{aligned} &\nabla_d \cdot \left(\left(r\mathbf{I} + \tilde{\mathbf{m}}^{n+\frac{1}{2}} \otimes \tilde{\mathbf{m}}^{n+\frac{1}{2}} \right) \nabla_d p^{n+\frac{1}{2}} \right)_{i,j} \\ &= \frac{1}{h} \left((\tilde{m}_1^{n+\frac{1}{2}} \tilde{m}_1^{n+\frac{1}{2}} + r) p_x^{n+\frac{1}{2}} + (\tilde{m}_1^{n+\frac{1}{2}} \tilde{m}_2^{n+\frac{1}{2}}) p_y^{n+\frac{1}{2}} \right)_{i+\frac{1}{2},j} \\ &\quad - \frac{1}{h} \left((\tilde{m}_1^{n+\frac{1}{2}} \tilde{m}_1^{n+\frac{1}{2}} + r) p_x^{n+\frac{1}{2}} + (\tilde{m}_1^{n+\frac{1}{2}} \tilde{m}_2^{n+\frac{1}{2}}) p_y^{n+\frac{1}{2}} \right)_{i-\frac{1}{2},j} \end{aligned}$$

$$\begin{aligned}
& + \frac{1}{h} \left((\tilde{m}_2^{n+\frac{1}{2}} \tilde{m}_1^{n+\frac{1}{2}}) p_x^{n+\frac{1}{2}} + (\tilde{m}_2^{n+\frac{1}{2}} \tilde{m}_2^{n+\frac{1}{2}} + r) p_y^{n+\frac{1}{2}} \right)_{i,j+\frac{1}{2}} \\
& - \frac{1}{h} \left((\tilde{m}_2^{n+\frac{1}{2}} \tilde{m}_1^{n+\frac{1}{2}}) p_x^{n+\frac{1}{2}} + (\tilde{m}_2^{n+\frac{1}{2}} \tilde{m}_2^{n+\frac{1}{2}} + r) p_y^{n+\frac{1}{2}} \right)_{i,j-\frac{1}{2}} \\
= & \frac{1}{h^2} (\tilde{m}_1^{n+\frac{1}{2}} \tilde{m}_1^{n+\frac{1}{2}} + r)_{i+\frac{1}{2},j} (p_{i+1,j}^{n+\frac{1}{2}} - p_{i,j}^{n+\frac{1}{2}}) \\
& - \frac{1}{h^2} (\tilde{m}_1^{n+\frac{1}{2}} \tilde{m}_1^{n+\frac{1}{2}} + r)_{i-\frac{1}{2},j} (p_{i,j}^{n+\frac{1}{2}} - p_{i-1,j}^{n+\frac{1}{2}}) \\
& - \frac{1}{4h^2} (\tilde{m}_1^{n+\frac{1}{2}} \tilde{m}_2^{n+\frac{1}{2}})_{i-\frac{1}{2},j} (p_{i,j+1}^{n+\frac{1}{2}} + p_{i-1,j+1}^{n+\frac{1}{2}} - p_{i,j-1}^{n+\frac{1}{2}} - p_{i-1,j-1}^{n+\frac{1}{2}}) \\
& + \frac{1}{4h^2} (\tilde{m}_1^{n+\frac{1}{2}} \tilde{m}_2^{n+\frac{1}{2}})_{i+\frac{1}{2},j} (p_{i,j+1}^{n+\frac{1}{2}} + p_{i+1,j+1}^{n+\frac{1}{2}} - p_{i,j-1}^{n+\frac{1}{2}} - p_{i+1,j-1}^{n+\frac{1}{2}}) \\
& + \frac{1}{h^2} (\tilde{m}_2^{n+\frac{1}{2}} \tilde{m}_2^{n+\frac{1}{2}} + r)_{i,j+\frac{1}{2}} (p_{i,j+1}^{n+\frac{1}{2}} - p_{i,j}^{n+\frac{1}{2}}) \\
& - \frac{1}{h^2} (\tilde{m}_2^n \tilde{m}_2^{n+\frac{1}{2}} + r)_{i,j-\frac{1}{2}} (p_{i,j}^{n+\frac{1}{2}} - p_{i,j-1}^{n+\frac{1}{2}}) \\
& + \frac{1}{4h^2} (\tilde{m}_2^{n+\frac{1}{2}} \tilde{m}_1^{n+\frac{1}{2}})_{i,j+\frac{1}{2}} (p_{i+1,j+1}^{n+\frac{1}{2}} + p_{i+1,j}^{n+\frac{1}{2}} - p_{i-1,j+1}^{n+\frac{1}{2}} - p_{i-1,j}^{n+\frac{1}{2}}) \\
& - \frac{1}{4h^2} (\tilde{m}_2^{n+\frac{1}{2}} \tilde{m}_1^{n+\frac{1}{2}})_{i,j-\frac{1}{2}} (p_{i+1,j-1}^{n+\frac{1}{2}} + p_{i+1,j}^{n+\frac{1}{2}} - p_{i-1,j}^{n+\frac{1}{2}} - p_{i-1,j-1}^{n+\frac{1}{2}}).
\end{aligned}$$

¹⁶⁵ Then the resulting linear system of Eq. (17a) can be solved by applying a multigrid method[52].

Step 3. Solve the reaction diffusion equations for updating the conductance with the updated p^{n+1} as follows:

$$\begin{aligned}
\frac{m_1^{n+1} - m_1^n}{\Delta t} = & K \Delta_d m_1^{n+\frac{1}{2}} + C \left(\tilde{m}_1^{n+\frac{1}{2}} p_x^{n+\frac{1}{2}} + \tilde{m}_2^{n+\frac{1}{2}} p_y^{n+\frac{1}{2}} \right) p_x^{n+\frac{1}{2}} \\
& - \alpha |\tilde{\mathbf{m}}^{n+\frac{1}{2}}|^{2(\gamma-1)} m_1^{n+\frac{1}{2}} + \zeta \left(\tilde{m}_1^{n+\frac{1}{2}} \tilde{\phi}_x^{n+\frac{1}{2}} + \tilde{m}_2^{n+\frac{1}{2}} \tilde{\phi}_y^{n+\frac{1}{2}} \right) \tilde{\phi}_x^{n+\frac{1}{2}}, \tag{18a}
\end{aligned}$$

$$\begin{aligned}
\frac{m_2^{n+1} - m_2^n}{\Delta t} = & K \Delta_d m_2^{n+\frac{1}{2}} + C \left(\tilde{m}_1^{n+\frac{1}{2}} p_x^{n+\frac{1}{2}} + \tilde{m}_2^{n+\frac{1}{2}} p_y^{n+\frac{1}{2}} \right) p_y^{n+\frac{1}{2}} \\
& - \alpha |\tilde{\mathbf{m}}^{n+\frac{1}{2}}|^{2(\gamma-1)} m_2^{n+\frac{1}{2}} + \zeta \left(\tilde{m}_1^{n+\frac{1}{2}} \tilde{\phi}_x^{n+\frac{1}{2}} + \tilde{m}_2^{n+\frac{1}{2}} \tilde{\phi}_y^{n+\frac{1}{2}} \right) \tilde{\phi}_y^{n+\frac{1}{2}}. \tag{18b}
\end{aligned}$$

¹⁶⁶ We should remark that Eqs. (18a) and (18b) can be solved by a biconjugate gradient coupled with a ¹⁶⁷ multigrid method for the resulting system of discrete equations[53, 54].

Step 4. Solve the Allen-Cahn type equation for updating the phase field with the updated \mathbf{m}^{n+1} and p^{n+1} as follows:

$$\begin{aligned}
\frac{\phi^{n+1} - \phi^n}{\Delta t} = & -\beta \frac{F'(\tilde{\phi}^{n+\frac{1}{2}})}{\epsilon^2} + \beta \Delta_d \phi^{n+\frac{1}{2}} + \zeta \left(\tilde{m}_1^{n+\frac{1}{2}} \tilde{m}_1^{n+\frac{1}{2}} \phi_x^{n+\frac{1}{2}} + \tilde{m}_1^{n+\frac{1}{2}} \tilde{m}_2^{n+\frac{1}{2}} \phi_y^{n+\frac{1}{2}} \right)_x \\
& + \zeta \left(\tilde{m}_2^{n+\frac{1}{2}} \tilde{m}_1^{n+\frac{1}{2}} \phi_x^{n+\frac{1}{2}} + \tilde{m}_2^{n+\frac{1}{2}} \tilde{m}_2^{n+\frac{1}{2}} \phi_y^{n+\frac{1}{2}} \right)_y, \tag{19}
\end{aligned}$$

¹⁶⁸ which can be solved by using the multigrid method.

¹⁶⁹ Some notations of the proposed method should be remarked here: (i) We use two level values, i.e., ϕ^{-1} ,

170 $\phi^0, \mathbf{m}^{-1}, \mathbf{m}^0, p^{-1}$ and p^0 , to initialize the computation. Let us set $\phi^{-1} := \phi^0, \mathbf{m}^{-1} := \mathbf{m}^0$ and $p^{-1} := p^0$,
 171 which will not reduce the accuracy of the numerical scheme. (ii) The diffusion term $D\Delta\mathbf{m}$ is stiff with
 172 a very small diffusion parameter D . However, we can manipulate it implicitly to increase the stability of
 173 the system because of the linearity of the Laplacian operator. (iii) The metabolism term $|\mathbf{m}|^{2(\gamma-1)}\mathbf{m}$ is
 174 nonlinear and non-differentiable for physical relevant cases $1/2 \leq \gamma \leq 1$, which is the metabolic rate of the
 175 bio-organism according to Murray's Law[29]. This activation term is stiff since $|\mathbf{m}|$ can be close to zero.
 176 Numerically, we add a small positive parameter $tol = 1e - 6$ as the stabilizer to avoid the zero denominator.
 177 (iv) The activation term is stiff with a large ∇p since the activation matrix $C(\nabla p \otimes \nabla p)$ has eigenvalues
 178 0 and $C|\nabla p|^2$. Using the currently-developed tricks for diffusion equations, such as linear penalization
 179 method, Newton iterations method, and Exponential Time Differencing method, will give rise to a nonlinear
 180 algebraic problem. In order to implement a practical algorithm with only linear algebraic complexity, we
 181 apply the preconditioned conjugate gradient method with the multigrid method as a preconditioner. Thus
 182 the computational complexity is $O(N)$, where $N = N_x \times N_y$ is the size of the mesh grid. (v) The central
 183 difference scheme is used for spatial discretization and the Crank-Nicolson type scheme is used for temporal
 184 discretization, which are both second-order accurate. (vi) The combination of the new decoupling method
 185 has the properties of linearity, unconditional energy stability and second-order accuracy, which is efficient
 186 and easy to implement.

187 3.2. Unconditional stability

In this subsection, we demonstrate the unconditional stability of the proposed scheme Eqs. (17). Let us
 define the modified energy as

$$\begin{aligned}
 & \tilde{\mathcal{E}}_d(\phi^{n+1}, \phi^n, \mathbf{m}^{n+1}, p^{n+1}) \\
 &= \mathcal{E}_d(\phi^{n+1}, \mathbf{m}^{n+1}, p^{n+1}) + \frac{\xi - F''(\sigma^{n,n+1})}{4\epsilon^2} \|\phi^{n+1} - \phi^n\|_d^2,
 \end{aligned} \tag{20}$$

where the discrete energy $\mathcal{E}_d(\phi^n, \mathbf{m}^n, p^n)$ is defined as:

$$\begin{aligned}
 \mathcal{E}_d(\phi^n, \mathbf{m}^n, p^n) &= \frac{K}{2} \|\nabla_d \mathbf{m}^n\|_d^2 + \frac{\alpha}{2\gamma} \|\mathbf{m}^n\|_d^{2\gamma} + \frac{C}{2} \|\mathbf{m}^n \cdot \nabla_d p^n\|_d^2 \\
 &+ \frac{Cr}{2} \|\nabla_d p^n\|_d^2 + \frac{\zeta}{2} \|\mathbf{m}^n \cdot \nabla_d \phi^n\|_d^2 + \beta \frac{F(\phi^n)}{\epsilon^2} + \frac{\beta}{2} \|\nabla_d \phi^n\|_d^2,
 \end{aligned} \tag{21}$$

and $\sigma^{n,n+1}$ satisfies the following functional:

$$\begin{aligned}
 & (F'(\tilde{\phi}^{n+\frac{1}{2}}), \phi^{n+1} - \phi^n)_d = (F(\phi^{n+1}) - F(\phi^n), 1)_d \\
 & - \frac{F''(\sigma^{n,n+1})}{4} (\|\phi^{n+1} - \phi^n\|_d^2 - \|\phi^n - \phi^{n-1}\|_d^2 + \|\phi^{n+1} - 2\phi^n + \phi^{n-1}\|_d^2).
 \end{aligned} \tag{22}$$

¹⁸⁸ Herein, we can provide the discrete energy dissipation law.

Theorem 3. The discrete system given in Eqs. (17) preserves the energy dissipation law as follows:

$$\begin{aligned} & \mathcal{E}_d(\phi^{n+1}, \phi^n, \mathbf{m}^{n+1}, p^{n+1}) - \mathcal{E}_d(\phi^n, \phi^{n-1}, \mathbf{m}^n, p^n) \\ &= -\|\mathbf{m}^{n+1} - \mathbf{m}^n\|_d^2/\Delta t - \|\phi^{n+1} - \phi^n\|_d^2/\Delta t - \beta \frac{\xi - F''(\sigma^{n+1,n})}{4\epsilon^2} \|\phi^{n+1} - 2\phi^n + \phi^{n-1}\|_d^2 \leq 0, \end{aligned}$$

¹⁸⁹ where ξ is the stabilizing parameter and satisfies $\xi \geq \max(F''(\phi)) = F''(\mathcal{G})$ with $|\phi| \leq \mathcal{G}$.

Proof. Let us compute the discrete inner product of Eqs. (17a)-(17c) with $\delta_t^+ p^n = (p^{n+1} - p^n)/\Delta t$, $\delta_t^+ \mathbf{m}^n = (\mathbf{m}^{n+1} - \mathbf{m}^n)/\Delta t$, and $\delta_t^+ \phi^n = (\phi^{n+1} - \phi^n)/\Delta t$, respectively:

$$\begin{aligned} -\|\delta_t^+ \mathbf{m}^n\|_d^2 &= \frac{K}{2} \delta_t^+ \|\mathbf{m}^n\|_d^2 + C \left(\mathbf{m}^{n+\frac{1}{2}} \cdot \nabla_d p^{n+\frac{1}{2}}, \delta_t^+ \mathbf{m}^n \nabla_d \tilde{p}^{n+\frac{1}{2}} \right)_d \\ &\quad + \alpha \left(\|\tilde{\mathbf{m}}^{n+\frac{1}{2}}\|_d^{2(\gamma-1)} \cdot \tilde{\mathbf{m}}^{n+\frac{1}{2}}, \delta_t^+ \mathbf{m}^n \right)_d - \left(\left(\mathbf{m}^{n+\frac{1}{2}} \nabla_d \phi^{n+\frac{1}{2}} \right) \cdot \nabla_d \tilde{\phi}^{n+\frac{1}{2}}, \delta_t^+ \mathbf{m}^n \right)_d, \end{aligned} \quad (23a)$$

$$\begin{aligned} -\|\delta_t^+ \phi^n\|_d^2 &= \frac{\beta}{\epsilon^2} \left(F' \left(\tilde{\phi}^{n+\frac{1}{2}} \right) + \xi \phi^{n+\frac{1}{2}} - \xi \tilde{\phi}^{n+\frac{1}{2}}, \delta_t^+ \phi^n \right)_d \\ &\quad + \beta \left(\nabla_d \phi^{n+\frac{1}{2}}, \nabla_d \delta_t^+ \phi^n \right)_d + \zeta \left(\left(\tilde{\mathbf{m}}^{n+\frac{1}{2}} \otimes \mathbf{m}^{n+\frac{1}{2}} \right) \nabla_d \phi^{n+\frac{1}{2}}, \nabla_d \delta_t^+ \phi^n \right)_d. \end{aligned} \quad (23b)$$

By combining Eq. (23a) and Eq. (23b), we can obtain the follows:

$$\begin{aligned} & -\|\delta_t^+ \mathbf{m}^n\|_d^2 - \|\delta_t^+ \phi^n\|_d^2 \\ &= C \left(r \nabla_d p^{n+\frac{1}{2}}, \nabla_d \delta_t^+ p^n \right)_d + \frac{K}{2} \delta_t^+ \|\mathbf{m}^n\|_d^2 \\ &\quad + C \left(\mathbf{m}^{n+\frac{1}{2}} \cdot \nabla_d p^{n+\frac{1}{2}}, \tilde{\mathbf{m}}^{n+\frac{1}{2}} \nabla_d \delta_t^+ p^n \right)_d + C \left(\mathbf{m}^{n+\frac{1}{2}} \cdot \nabla_d p^{n+\frac{1}{2}}, \delta_t^+ \mathbf{m}^n \nabla_d \tilde{p}^{n+\frac{1}{2}} \right)_d \\ &\quad + \alpha \left(|\tilde{\mathbf{m}}^{n+\frac{1}{2}}|^{2(\gamma-1)} \cdot \mathbf{m}^{n+\frac{1}{2}}, \delta_t^+ \mathbf{m}^n \right)_d - \zeta \left(\left(\mathbf{m}^{n+\frac{1}{2}} \nabla_d \phi^{n+\frac{1}{2}} \right) \cdot \nabla_d \tilde{\phi}^{n+\frac{1}{2}}, \delta_t^+ \mathbf{m}^n \right)_d \\ &\quad + \frac{\beta}{\epsilon^2} \left(F' \left(\tilde{\phi}^{n+\frac{1}{2}} \right) + \xi \phi^{n+\frac{1}{2}} - \xi \tilde{\phi}^{n+\frac{1}{2}}, \delta_t^+ \phi^n \right)_d + \beta \left(\nabla_d \phi^{n+\frac{1}{2}}, \nabla_d \delta_t^+ \phi^n \right)_d \\ &\quad + \zeta \left(\left(\tilde{\mathbf{m}}^{n+\frac{1}{2}} \otimes \mathbf{m}^{n+\frac{1}{2}} \right) \nabla_d \phi^{n+\frac{1}{2}}, \nabla_d \delta_t^+ \phi^n \right)_d, \end{aligned}$$

where we have

$$\begin{aligned} & \left(\left(\tilde{\mathbf{m}}^{n+\frac{1}{2}} \otimes \mathbf{m}^{n+\frac{1}{2}} \right) \nabla_d \phi^{n+\frac{1}{2}}, \nabla_d \delta_t^+ \phi^n \right)_d - \left(\left(\mathbf{m}^{n+\frac{1}{2}} \nabla_d \phi^{n+\frac{1}{2}} \right) \cdot \nabla_d \tilde{\phi}^{n+\frac{1}{2}}, \delta_t^+ \mathbf{m}^n \right)_d \\ &= \left(\mathbf{m}^{n+\frac{1}{2}} \nabla_d \phi^{n+\frac{1}{2}}, \delta_t^+ \mathbf{m}^n \cdot \nabla_d \tilde{\phi}^{n+\frac{1}{2}} \right)_d + \left(\mathbf{m}^{n+\frac{1}{2}} \nabla_d \phi^{n+\frac{1}{2}}, \tilde{\mathbf{m}}^{n+\frac{1}{2}} \nabla_d \delta_t^+ \phi^n \right)_d. \end{aligned}$$

Note that we can consider the reformulation as the following parts:

$$\left(\mathbf{m}^{n+\frac{1}{2}} \cdot \nabla_d p^{n+\frac{1}{2}}, \tilde{\mathbf{m}}^{n+\frac{1}{2}} \nabla_d \delta_t^+ p^n \right)_{L_2} + \left(\mathbf{m}^{n+\frac{1}{2}} \cdot \nabla_d p^{n+\frac{1}{2}}, \delta_t^+ \mathbf{m}^n \nabla_d \tilde{p}^{n+\frac{1}{2}} \right)_d$$

$$\begin{aligned}
&= \left(\mathbf{m}^{n+\frac{1}{2}} \cdot \nabla_d p^{n+\frac{1}{2}}, \tilde{\mathbf{m}}^{n+\frac{1}{2}} \nabla_d \delta_t^+ p^n + \delta_t^+ \mathbf{m}^n \nabla_d \tilde{p}^{n+\frac{1}{2}} \right)_d \\
&= \left(\mathbf{m}^{n+\frac{1}{2}} \cdot \nabla_d p^{n+\frac{1}{2}}, \delta_t^+ (\mathbf{m}^n \cdot \nabla_d p^n) \right)_d = \frac{1}{2} \delta_t^+ \|\mathbf{m}^n \cdot \nabla_d p^n\|_d^2,
\end{aligned}$$

and

$$\begin{aligned}
&\left(\alpha \|\tilde{\mathbf{m}}^{n+\frac{1}{2}}\|_d^{2(\gamma-1)} \cdot \tilde{\mathbf{m}}^{n+\frac{1}{2}}, \delta_t^+ \mathbf{m}^n \right)_d = \left(\alpha \|\tilde{\mathbf{m}}^{n+\frac{1}{2}}\|_d^{\gamma-2} \cdot \tilde{\mathbf{m}}^{n+\frac{1}{2}} \cdot \|\mathbf{m}^{n+\frac{1}{2}}\|_d^\gamma, \delta_t^+ \mathbf{m}^n \right)_d \\
&= \left(\|\mathbf{m}^{n+\frac{1}{2}}\|_d^\gamma, \alpha \|\tilde{\mathbf{m}}^{n+\frac{1}{2}}\|_d^{\gamma-2} \cdot \tilde{\mathbf{m}}^{n+\frac{1}{2}} \cdot \delta_t^+ \mathbf{m}^n \right)_d = \left(\|\mathbf{m}^{n+\frac{1}{2}}\|_d^\gamma, \delta_t^+ \|\mathbf{m}^n\|_d^\gamma \right)_d = \frac{1}{2} \delta_t^+ \|\mathbf{m}^n\|_d^2.
\end{aligned}$$

For the term $\left((F'(\tilde{\phi}^{n+\frac{1}{2}}) + \xi \phi^{n+\frac{1}{2}} - \xi \tilde{\phi}^{n+\frac{1}{2}})/\epsilon^2, \delta_t^+ \phi^n \right)_d$, we get

$$\begin{aligned}
&\frac{1}{\epsilon^2} \left(F'(\tilde{\phi}^{n+\frac{1}{2}}) + \xi \phi^{n+\frac{1}{2}} - \xi \tilde{\phi}^{n+\frac{1}{2}}, \delta_t^+ \phi^n \right)_d \\
&= \frac{1}{\epsilon^2} \left(F'(\tilde{\phi}^{n+\frac{1}{2}}), \delta_t^+ \phi^n \right)_d + \frac{1}{\epsilon^2} \left(\xi \phi^{n+\frac{1}{2}} - \xi \tilde{\phi}^{n+\frac{1}{2}}, \delta_t^+ \phi^n \right)_d \\
&= \frac{1}{\Delta t \epsilon^2} \left(F(\phi^{n+1}) - F(\phi^n), 1 \right)_d \\
&\quad + \frac{F''(\sigma^{n+1,n})}{4\epsilon^2} (\|\phi^n - \phi^{n-1}\|_d^2 - \|\phi^{n+1} - \phi^n\|_d^2 - \|\phi^{n+1} - 2\phi^n + \phi^{n-1}\|_d^2) \\
&\quad + \frac{\xi}{4\epsilon^2 \Delta t} (\|\phi^{n+1} - \phi^n\|_d^2 - \|\phi^n - \phi^{n-1}\|_d^2 + \|\phi^{n+1} - 2\phi^n + \phi^{n-1}\|_d^2) \\
&= \frac{1}{\Delta t \epsilon^2} \left(F(\phi^{n+1}) - F(\phi^n), 1 \right)_d + \frac{\xi - F''(\mathcal{G})}{4\epsilon^2 \Delta t} \|\phi^{n+1} - 2\phi^n + \phi^{n-1}\|_d^2.
\end{aligned}$$

Here, the function $\sigma^{n+1,n}$ exists because of the Taylor expansion. Since the mean value theorem of integral, there exists $\mathcal{G} \in [\phi^n, \phi^{n+1}]$. Therefore, we can obtain

$$\begin{aligned}
&- \|\delta_t^+ \mathbf{m}^n\|_d^2 - \|\delta_t^+ \phi^n\|_d^2 \\
&= \frac{K}{2} \delta_t^+ \|\mathbf{m}^n\|_d^2 + \frac{C}{2} \delta_t^+ \|\mathbf{m}^n \cdot \nabla_d p^n\|_d^2 + \frac{1}{2} C r \delta_t^+ \|p^n\|_d^2 \\
&\quad + \frac{\alpha}{2r} \delta_t^+ \|\mathbf{m}^n\|_d^2 + \frac{\zeta}{2} \delta_t^+ \|\mathbf{m}^n \cdot \nabla_d \phi^n\|_d^2 + \frac{\beta}{\Delta t \epsilon^2} \left(F(\phi^{n+1}) - F(\phi^n), 1 \right)_d \\
&\quad + \frac{1}{2} \delta_t^+ \|\phi^n\|_d^2 + \beta \frac{\xi - F''(\sigma^{n+1,n})}{4\epsilon^2 \Delta t} \|\phi^{n+1} - 2\phi^n + \phi^{n-1}\|_d^2.
\end{aligned} \tag{24}$$

Let us consider

$$\begin{aligned}
&\mathcal{E}_d(p^{n+1}, \mathbf{m}^{n+1}, \phi^{n+1}) - \mathcal{E}_d(p^n, \mathbf{m}^n, \phi^n) \\
&= \left(\mathcal{E}_d(p^{n+1}, \mathbf{m}^{n+1}, \phi^{n+1}) - \mathcal{E}_d(p^{n+1}, \mathbf{m}^{n+1}, \phi^n) \right) + \left(\mathcal{E}_d(p^{n+1}, \mathbf{m}^{n+1}, \phi^n) \right. \\
&\quad \left. - \mathcal{E}_d(p^{n+1}, \mathbf{m}^n, \phi^n) \right) + \left(\mathcal{E}_d(p^{n+1}, \mathbf{m}^n, \phi^n) - \mathcal{E}_d(p^n, \mathbf{m}^n, \phi^n) \right),
\end{aligned} \tag{25}$$

where we have the following parts:

$$\begin{aligned} & \mathcal{E}_d(p^{n+1}, \mathbf{m}^n, \phi^n) - \mathcal{E}_d(p^n, \mathbf{m}^n, \phi^n) \\ &= \frac{C}{2} (\mathbf{m}^n \otimes \mathbf{m}^n) (\|\nabla_d p^{n+1}\|_d^2 - \|\nabla_d p^n\|_d^2) + \frac{Cr}{2} (\|\nabla_d p^{n+1}\|_d^2 - \|\nabla_d p^n\|_d^2), \end{aligned} \quad (26)$$

and

$$\begin{aligned} & \mathcal{E}_d(p^{n+1}, \mathbf{m}^{n+1}, \phi^n) - \mathcal{E}_d(p^{n+1}, \mathbf{m}^n, \phi^n) \\ &= \frac{K}{2} (\|\nabla_d \mathbf{m}^{n+1}\|_d^2 - \|\nabla_d \mathbf{m}^n\|_d^2) + \frac{\alpha}{2r} (\|\mathbf{m}^{n+1}\|_d^2 - \|\mathbf{m}^n\|_d^2) \\ &\quad + \frac{C}{2} (\|\mathbf{m}^{n+1} \nabla_d p^{n+1}\|_d^2 - \|\mathbf{m}^n \nabla_d p^n\|_d^2) + \frac{\zeta}{2} (\|\mathbf{m}^{n+1} \nabla_d \phi^{n+1}\|_d^2 - \|\mathbf{m}^n \nabla_d \phi^n\|_d^2), \end{aligned} \quad (27)$$

and

$$\begin{aligned} & \mathcal{E}_d(p^{n+1}, \mathbf{m}^{n+1}, \phi^{n+1}) - \mathcal{E}_d(p^{n+1}, \mathbf{m}^{n+1}, \phi^n) \\ &= \frac{\beta}{\epsilon^2} (F(\phi^{n+1}) - F(\phi^n), 1)_d + \frac{\beta}{2} (\|\nabla_d \phi^{n+1}\|_d^2 - \|\nabla_d \phi^n\|_d^2) + \frac{\zeta}{2} \|\mathbf{m}^{n+1} \nabla_d \phi^{n+1}\|_d^2 - \frac{\zeta}{2} \|\mathbf{m}^n \nabla_d \phi^n\|_d^2. \end{aligned} \quad (28)$$

By combining Eqs. (26)-(28), we get

$$\begin{aligned} & \mathcal{E}_d(p^{n+1}, \mathbf{m}^{n+1}, \phi^{n+1}) - \mathcal{E}_d(p^n, \mathbf{m}^n, \phi^n) \\ &= \frac{C}{2} (\mathbf{m}^n \otimes \mathbf{m}^n) (\|\nabla_d p^{n+1}\|_d^2 - \|\nabla_d p^n\|_d^2) \\ &\quad + \frac{Cr}{2} (\|\nabla_d p^{n+1}\|_d^2 - \|\nabla_d p^n\|_d^2) + \frac{K}{2} (\|\nabla_d \mathbf{m}^{n+1}\|_d^2 - \|\nabla_d \mathbf{m}^n\|_d^2) \\ &\quad + \frac{\alpha}{2r} (\|\mathbf{m}^{n+1}\|_d^2 - \|\mathbf{m}^n\|_d^2) + \frac{C}{2} (\|\mathbf{m}^{n+1} \nabla_d p^{n+1}\|_d^2 - \|\mathbf{m}^n \nabla_d p^n\|_d^2) \\ &\quad + \frac{\zeta}{2} (\|\mathbf{m}^{n+1} \nabla_d \phi^{n+1}\|_d^2 - \|\mathbf{m}^n \nabla_d \phi^n\|_d^2) + \frac{\beta}{\epsilon^2} (F(\phi^{n+1}) - F(\phi^n), 1)_d \\ &\quad + \frac{\beta}{2} (\|\nabla_d \phi^{n+1}\|_d^2 - \|\nabla_d \phi^n\|_d^2) + \frac{\zeta}{2} (\|\mathbf{m}^{n+1} \nabla_d \phi^{n+1}\|_d^2 - \|\mathbf{m}^n \nabla_d \phi^n\|_d^2) \\ &= -\|\mathbf{m}^{n+1} - \mathbf{m}^n\|_d^2 / \Delta t - \|\phi^{n+1} - \phi^n\|_d^2 / \Delta t - \beta \frac{\xi - F''(\sigma^{n+1,n})}{4\epsilon^2} \|\phi^{n+1} - 2\phi^n + \phi^{n-1}\|_d^2 \leq 0. \end{aligned}$$

190 Here the proof is completed. \square

191 **Remark 1.** Since \mathbf{m} is coupled with ϕ in Eq. (12a) and $F(\phi)$ exhibits quartic growth at infinity, we cannot
192 prove analytically that ϕ is bounded. However, we should point out that ϕ can be verified to be bounded
193 numerically with the initial condition $\phi^0 \in [0, 1]$. Meanwhile, considering that the original Allen-Cahn
194 equation is restricted to satisfy the maximum principle according to the existing discussions, we assume
195 that there exists \mathcal{G} , which is not-significantly larger than 1, to satisfy $\phi \leq \mathcal{G}$.

196 There are also other efficient algorithms, such as the iterative threshold dynamics method[55], invariant
 197 energy quadratization method[56, 57], scalar auxiliary variable method[58], to solve the reaction-type model.
 198 Our proposed method performs a straightforward strategy to prove the energy dissipation law. Furthermore,
 199 in order to match the theoretical proof of energy dissipation, we adopt the above algorithm. We should take
 200 some notations: (i) We provide a novel theoretical proof for the modified model coupled with the phase field,
 201 and guarantee the corresponding energy functional conservation. (ii) Our semi-implicit discrete algorithm is
 202 composed by several linear equations, which can be solved by using several fast numerical procedures with
 203 linear algebraic computational complexity.

204 4. Numerical experiments

205 Several numerical tests have been performed such as the energy dissipation test, stability test, the
 206 convergence test, the comparison test with different initial conditions of conductivity, and three dimensional
 207 test. Throughout this paper, we choose the computational domain as $\Omega = [-1, 1] \times [-1, 1]$ with a 512×512
 208 mesh-grid and use the following parameters for the numerical simulations: $\epsilon = 5h/(4\sqrt{2}\text{atanh}(0.9))$, $r = 0.1$,
 209 $C = 50^2$, $K = 0.005^2$, $\alpha = 1$, $\gamma = 0.75$, $\beta = 0.01$, $\zeta = 0.05$, $\xi = 0.5$ and $\Delta t = 0.8h$.

210 4.1. Non-increasing discrete energy test

We study the temporal evolution of the normalized discrete energy $\mathcal{E}_d(\phi^n)/\mathcal{E}_d(\phi^0)$. The initial conditions

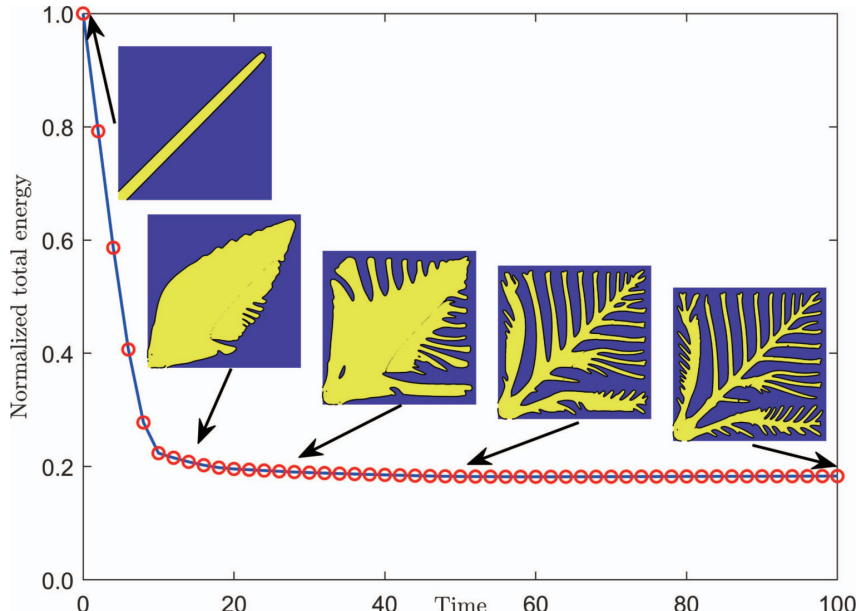


Figure 1: Temporal evolution of the non-increasing energy of the proposed model. Note that the modified energy has been normalized by the initial energy. The inset figures are the morphology of phase field ϕ in the L_2 space at specific times $t = 0, 12.5, 25, 50$, and 100 , respectively.

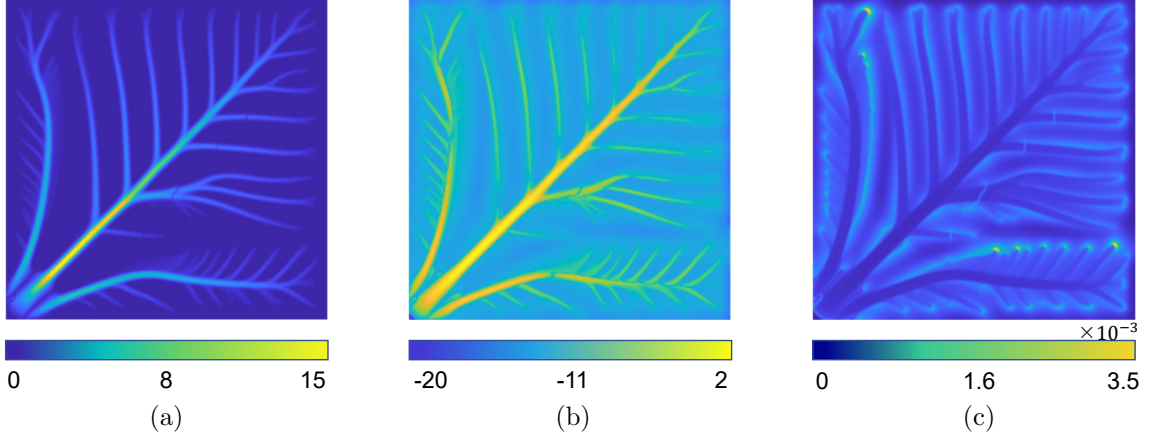


Figure 2: From (a) to (c), the results are the L_2 norm of conductance vector \mathbf{m} , the L_2 norm of fluid velocity \mathbf{v} in the log scale, and the L_2 norm of the gradient of pressure ∇p at the final time of Fig. 1, respectively.

are chosen as follows:

$$\phi(x, y, 0) = 0.5 - 0.5 \tanh \left(\frac{(|y - x| - 0.075, |x - y| - 0.075)}{2\sqrt{2}\epsilon} \right), \quad (29a)$$

$$\mathbf{m}(x, y, 0) = \left(0.5\phi(x, y, 0)(4 - |x| - |y|), 0.2\phi(x, y, 0)(4 - |x| - |y|) \right), \quad (29b)$$

$$p(x, y, 0) = 0, \quad S(x, y, 0) = 1 - \tanh \left(\frac{\sqrt{(y - 0.15)^2 + (x - 0.15)^2} - 0.15}{2\sqrt{2}\epsilon} \right). \quad (29c)$$

The procedure has been applied until $T = 100$. The inset figures are the morphology of the phase field at indicated times $t = 0, 12.5, 25, 50$, and 100 , respectively. The modified total energy has been normalized by the initial energy. The results shown in Fig. 1 suggest that the discrete total energy has decayed unconditionally. As can be seen from the evolution of the generating process, the leaf shape is formed under the influence of the diffusion of electrical conductivity on the trunk. The tree-like biological network has generated while branches are formed from the trunk and the ablations appear on the tissue between the branches. We note that the subfigures in Fig. 1 demonstrate the stationary results of the biological network, which keeps the structure when further evolving. We have used the same initial conditions as Eqs. (29) and plotted the contour figures results in Fig. 2 to show the L_2 norm of different physical properties, such as conductance vector \mathbf{m} , fluid velocity \mathbf{v} in the log scale, and the gradient of pressure ∇p , respectively. We introduced the coupled term $(\mathbf{m} \cdot \nabla \phi)\nabla \phi$ in to the governing equations, which can help to stabilize the boundaries between venation phase and tissue phase and improve the stability of numerical schemes. As can be seen from Fig. 2(a), the leaf venation grows as the fluid spreads, and finally achieves a tree-like structure. By considering Fig. 2(b), we can see that the velocity value of venation phase is larger than that of tissue phase, which is influenced by the osmotic pressure on phase boundary as shown in Fig. 2(c). The coupling

term is directly suppress the transport perpendicular to the phase boundaries, while has less influence on the internal transmission.

4.2. Effect of the phase boundaries

The coupling term composed by \mathbf{m} and ϕ in the governing equations Eqs. (12) is directly suppress the transport perpendicular to the phase boundaries. Considering that the pressure variable p is a passive

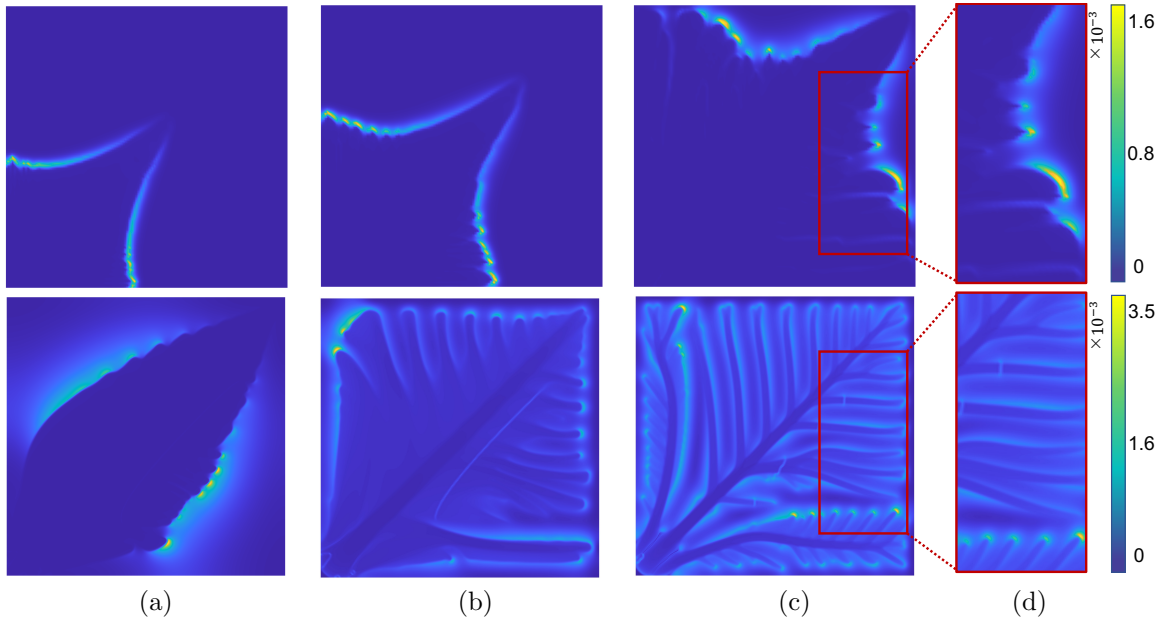


Figure 3: The dynamical behaviors of $\|\nabla p\|_{L_2}$ with the original model Eqs. (5)(Top row) and the modified model Eqs. (12)(Bottom row). From (a) to (c), the results are the contour figures of $\|\nabla p\|_{L_2}$ captured at the indicated times 12.5, 50, and 100, respectively. (d) is the close view of (c).

quantity[59] caused by the dynamical behaviors of the conductance \mathbf{m} , whose gradient ∇p coincides with the transport direction perpendicularly to the phase boundary. Furthermore, the modulus of ∇p indicates how strongly the tissue passes through the boundaries. In order to demonstrate the inhibition caused by the introduced phase field, we design a comparison numerical test to consider the norm of the interfacial pressure gradient of the original model Eqs. (5) and the modified model Eqs. (12) respectively. The contour results of $\|\nabla p\|_{L_2}$ in the two cases at different indicated times 12.5, 50, and 100 are shown in Fig. 3. As can be seen, under the inhibition effect brought by performing the phase field coupling term, the norm of ∇p becomes large, which implies that it is difficult for the venation to cross phase boundaries. In other words, the introduction of phase field model makes branches easier to be formed from the trunk.

4.3. Stability test

Since our model contains the strong nonlinear term and high order spatial derivatives, i.e. the convention term and the chemical potential term respectively, the explicit time scheme results in severe time-step

restrictions for stability. To demonstrate the stability of our proposed scheme, we perform the numerical experiment with $\Delta t = 5, 0.5, 0.05$ and 0.005 , respectively. The initial conditions are set as

$$\phi(x, y, 0) = 1 - \tanh\left(\frac{\sqrt{(y - 0.15)^2 + (x - 0.15)^2} - 0.15}{2\sqrt{2}\epsilon}\right), \quad (30a)$$

$$m_1(x, y, 0) = \phi(x, y, 0), \quad m_2(x, y, 0) = 0.5\phi(x, y, 0), \quad (30b)$$

$$S(x, y, 0) = \phi(x, y, 0), \quad p(x, y, 0) = 0. \quad (30c)$$

The chosen parameters are the same as those in Section 4.1. As can be seen from Fig. 4, we compare

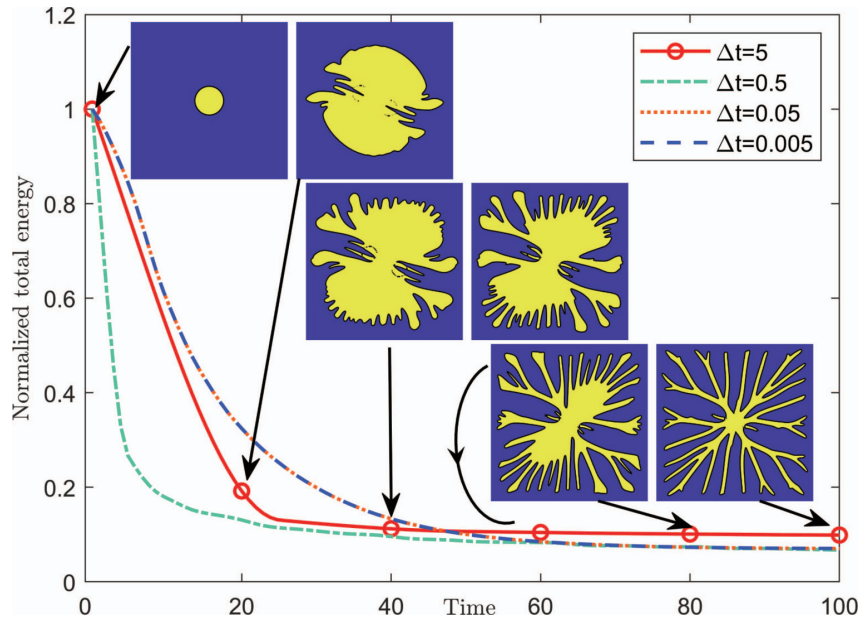


Figure 4: Temporal evolution of the energy functional of the proposed model with four time step sizes of $\Delta t = 5, 0.5, 0.05$, and 0.005 until $T = 100$, respectively. Note that the modified energy has been normalized by the initial energy. The inset figures are the morphology of the phase field ϕ in the L_2 space at specific times $t = 0, 20, 40, 60, 80$, and 100 , respectively. The subfigures are obtained with $\Delta t = 5$.

241
242 the temporal evolution of the total energy with four different time steps $\Delta t = 5, 0.5, 0.05$ and 0.005 until
243 $t = 100$. It is obvious that the four energy curves decay unconditionally and no blow-up of the numerical
244 solutions occur, which indicate that the large time steps can be used for the investigation of our method.
245 Furthermore, we can obviously see that the results with $\Delta t = 0.05$ are in good agreement with results
246 obtained by using $\Delta t = 0.005$ while differ from the results with the larger time step $\Delta t = 5$. As can be
247 seen from this figure, using the small time step can obtain more accurate results than those with large time
248 step since large truncation errors of the numerical solutions cannot be avoided. Thus, in order to obtain the
249 higher accurate numerical solutions, a small time step should be used for further computation. In this paper,
250 we suggest performing the numerical scheme with an appropriate value $\Delta t = 0.005$ to maintain our proposed
251 scheme's accuracy and reduce computational costs. The inset figures in Fig. 4 are the morphology of the

252 phase field with $\Delta t = 5$ at indicated times 0, 20, 40, 60, 80, and 100, respectively. As can be seen from the
 253 evolution of the network generation, the diffusion effect is dominant in the early stage of energy dissipation.
 254 The cross term plays the dominant role in the process of gradual stabilization with the nutrients ablation
 255 between the branches to ensure network connectivity. The evolution of the network generation indicates
 256 that the numerical solutions are convergent and the large time steps can be used. In order to demonstrate
 257 that the phase field is bounded, we have captured the contour figure of the dynamical behaviors with the
 258 same initial conditions of Eqs. (30) at the indicated times 20, 60, and 100, respectively. We have added the
 259 top slice($z = 1$) and bottom slice($z = 0$) in the subfigures to show the supremum and infimum of phase field.
 260 As can be seen from the results, the introduced phase variables are indeed bounded, which corresponds to
 261 our expectations.

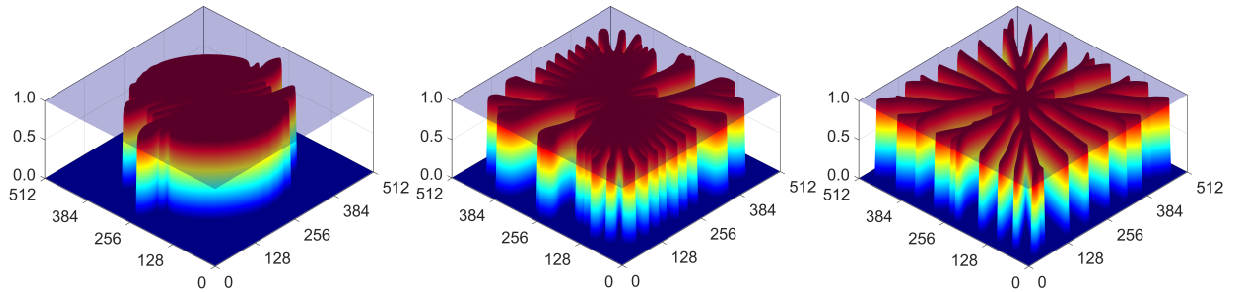


Figure 5: The dynamical behaviors of the phase field with the same initial conditions of Eqs. (30). From left to right, the indicated times are 20, 60, and 100, respectively. The top slice($z = 1$) and bottom slice($z = 0$) of every sub figures are the supremum and infimum of phase field.

262 4.4. Convergence test

In order to examine the numerical accuracy of the proposed method, we perform the following Euler method in domain $\Omega = [0, 2] \times [0, 2]$. Since no closed-form analytical solution exists for the proposed method, we denote the following reference solution ϕ^{ref} , m_1^{ref} , m_2^{ref} and p^{ref} , which can be obtained by the fine time step or the fine grid size for the investigation of spatial accuracy and temporal accuracy, respectively. Let us set the initial conditions as follows:

$$\begin{aligned}
 \phi(x, y, 0) &= \sin(\pi x) \cos(\pi y), & p(x, y, 0) &= \cos(\pi x) \sin(\pi y), \\
 m_1(x, y, 0) &= \sin(\pi x) \sin(\pi y), & m_2(x, y, 0) &= \cos(\pi x) \cos(\pi y), \\
 S(x, y, 0) &= 1 - \tanh\left(\frac{\sqrt{(y - 0.15)^2 + (x - 0.15)^2} - 0.15}{2\sqrt{2}\epsilon}\right).
 \end{aligned}$$

263 The homogeneous Neumann boundary conditions have been applied for the convergence test. We first use
 264 the decreasing temporal steps as $\Delta t = 1.6\text{e-}4$, $\Delta t = 8.0\text{e-}5$, and $\Delta t = 4.0\text{e-}5$ with the fine spatial size
 265 $h = 1/512$, respectively, to investigate the second-order temporal accuracy. Let us define the reference

266 solutions as the results obtained by using $\Delta t = 1.0e-5$, which indicates that the numerical error is defined as
 267 $e_{i,\Delta t} := \phi_{i,\Delta t} - \phi_i^{\text{ref}}$. Thus the convergence rate can be defined as $\log_2(||e_{i,\Delta t}||_2 / ||e_{i,\Delta t/2}||_2)$. The numerical
 268 error and convergence rate have been listed in Table 1, which indicates numerically that our proposed
 method has second-order temporal accuracy corresponding to system Eqs. (17). Then we perform the fixed

Table 1: Errors and convergence rates with different time steps for the conductance m_1 and m_2 , pressure p and phase field ϕ .

Δt	Error				Order			
	m_1	m_2	p	ϕ	m_1	m_2	p	ϕ
1.6e - 4	6.342e - 04	5.162e - 04	4.153e - 04	8.819e - 04	—	—	—	—
8.0e - 5	1.506e - 04	1.155e - 04	1.072e - 04	1.951e - 04	2.07	2.16	1.95	2.18
4.0e - 5	3.906e - 05	2.731e - 05	2.546e - 05	4.753e - 05	1.95	2.08	2.07	2.04

269
 270 temporal step size $\Delta t = 1.0e-5$ to investigate the spatial convergence rate until $T = 0.1$. Let us consider
 271 the decreasing spatial steps as $h = 1/128$, $h = 1/256$, and $h = 1/512$, respectively. Let us define the spatial
 272 error as $e_{i,h} := \phi_{i,h} - \phi_i^{\text{ref}}$ and define the spatial convergence rate as $\log_2(||e_{i,h}||_2 / ||e_{i,h/2}||_2)$, where the
 273 reference solution is obtained by using the fine space grid size $h = 1/1024$. The numerical errors and spatial
 274 convergence results are listed in Table 2, which indicate that our proposed method is second-order accurate
 275 in space.

Table 2: Errors and convergence rates with different spatial steps for the conductance m_1 and m_2 , pressure p , and phase field ϕ .

N	Error				Order			
	m_1	m_2	p	ϕ	m_1	m_2	p	ϕ
128	8.572e - 03	7.273e - 03	6.249e - 03	7.114e - 03	—	—	—	—
256	2.021e - 03	1.749e - 03	1.416e - 03	1.635e - 03	2.08	2.06	2.14	2.12
512	5.384e - 04	4.224e - 04	3.139e - 04	4.202e - 04	1.92	2.05	2.17	1.96

276 4.5. Presentation of various classical biological network generation

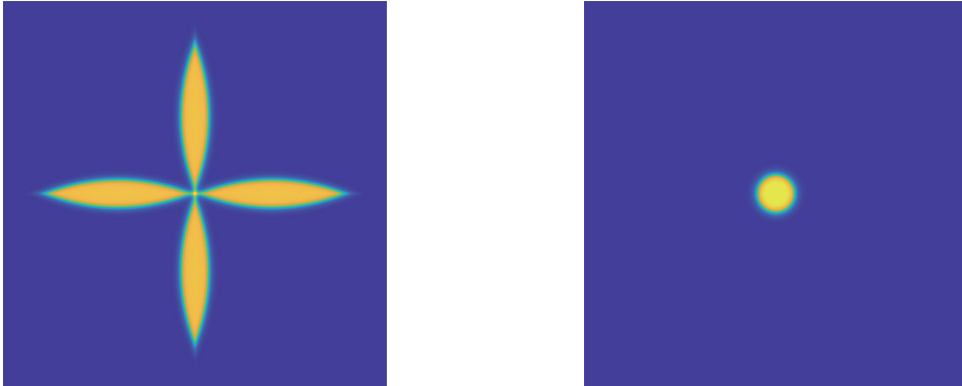


Figure 6: Schematic illustration of the initial conditions. (a) is the initial conductance $m_1(x, y, 0)$. (b) is the source term $S(x, y)$.

In this subsection, we perform the comparison test with different initial conditions to verify the influence of initial conditions on the generation of biological neural networks. The value of m_1 for three comparative experiments is set to be the same with the different values of m_2 . The initial conditions are chosen as follows:

$$\begin{aligned}\phi(x, y, 0) &= 2 - 0.5 \tanh \left(\left(|x - 0.5| + (y - 0.25)^2 - 0.03 \right) / \sqrt{5\epsilon} \right) \\ &\quad - 0.5 \tanh \left(\left((x - 0.25)^2 + |y - 0.5| - 0.03 \right) / \sqrt{5\epsilon} \right) \\ &\quad - 0.5 \tanh \left(\left(|x - 0.5| + (y - 0.75)^2 - 0.03 \right) / \sqrt{5\epsilon} \right) \\ &\quad - 0.5 \tanh \left(\left((x - 0.75)^2 + |y - 0.5| - 0.03 \right) / \sqrt{5\epsilon} \right) \\ S(x, y, 0) &= 1 - \tanh \left(\left(\sqrt{(y - 0.5)^2 + (x - 0.5)^2} - 0.15 \right) / 2\sqrt{2\epsilon} \right), \\ m_1(x, y, 0) &= \phi(x, y, 0), \quad p(x, y, 0) = 0, \\ m_{2a}(x, y, 0) &= 0, \quad m_{2b}(x, y, 0) = 0.5\phi(x, y, 0), \quad m_{2c}(x, y, 0) = \phi(x, y, 0),\end{aligned}$$

which can be shown in Fig. 6. Before we proceed the investigation on the comparative tests, let us define another variable of interest in the model as the volumetric flux \mathbf{v} , which is proportional to the flow velocity in the biological tissue and can be defined by $\mathbf{v} = -(r\mathbf{I} + \mathbf{m} \otimes \mathbf{m})\nabla p$. The long-time behavior of the solutions has been shown in Fig. 7. The first column demonstrates the norm of the conductance \mathbf{m} , the second column demonstrates the norm of the volumetric flux \mathbf{v} , and the last column demonstrates the energy dissipation of the total energy by the proposed method. As can be seen from the last column, the normalized total energy is decreasing. It is obvious that the adjustment of initial condition will only influence the degree of energy dissipation rather than the trend of unconditional dissipation. Furthermore, we can see that there are bifurcations only at the boundary of the capillary duct and differences at the junction of the branches. We note that the difference of the initial \mathbf{m} can lead to an anisotropic distribution of conductivity, which is concentrated on the location of the source term. We have to emphasize that the initial value should not have drastic effects on the generation of biological networks, except for minor changes in the capillary channels.

4.6. Three dimensional test

In this subsection, we apply the phase field based biological network generation procedure in three dimension as shown in Fig. 8. The computational domain is chosen as $\Omega = [-1, 1] \times [-1, 1] \times [-1, 1]$ with the $128 \times 128 \times 128$ mesh grid. The initial conditions are chosen as

$$\begin{aligned}\phi(x, y, 0) &= 0.5 - 0.5 \tanh \left(\frac{\left(|x - y| - 0.075, |y - z| - 0.075, |z - x| - 0.075 \right)}{2\sqrt{2\epsilon}} \right), \\ \mathbf{m}(x, y, 0) &= (5, 2, 1)\phi(x, y, 0)\left(4 - |x| - |y| - |z|\right), \quad p(x, y, 0) = 0,\end{aligned}$$

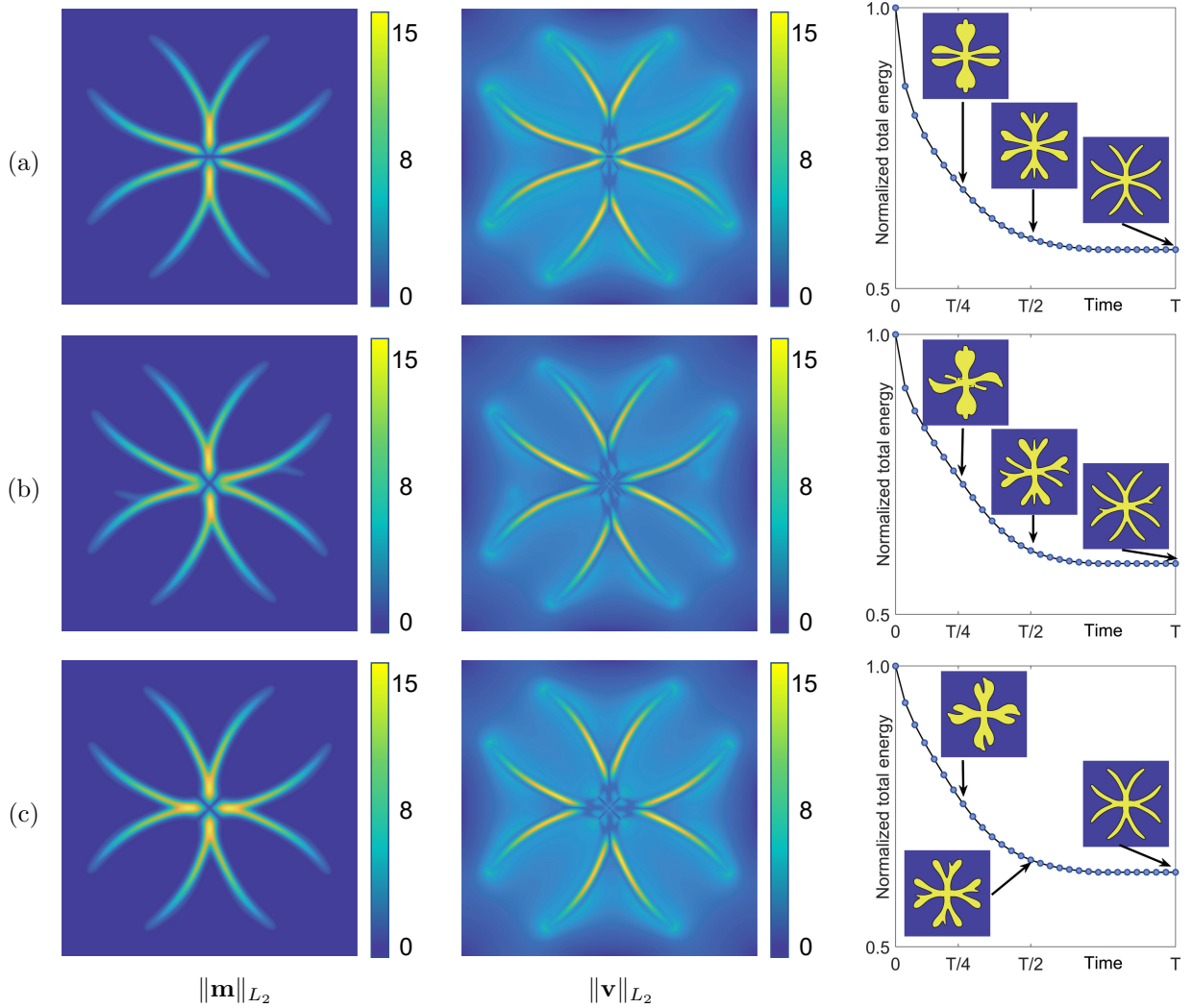


Figure 7: Temporal evolution of $\|\mathbf{m}\|_{L_2}$, $\|\mathbf{v}\|_{L_2}$, and the discrete energy with different values of m_2 . Note that the modified energy has been normalized by the initial energy.

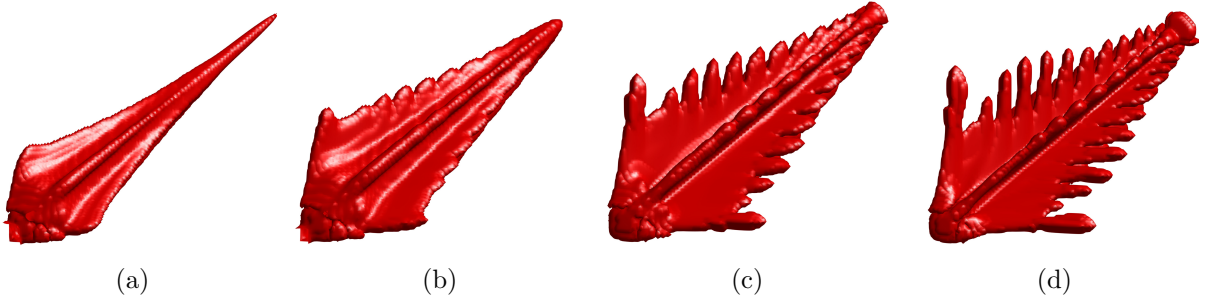


Figure 8: The morphology of the phase field during the generation of biological transport network in three dimension. From (a) to (d), the indicated times are $t = 5, 10, 20$ and 40 , respectively.

$$S(x, y, 0) = 1 - \tanh \left(\frac{\sqrt{(x - 0.15)^2 + (y - 0.15)^2 + (z - 0.15)^2} - 0.12}{2\sqrt{2}\epsilon} \right).$$

As can be seen from Fig. 8(a) to (d), we demonstrate the dynamical behaviors of the biological generation

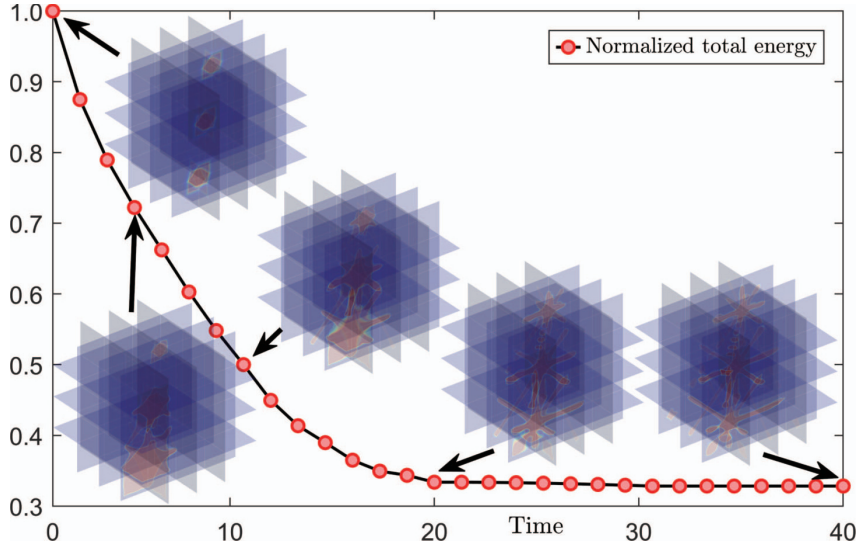


Figure 9: Temporal evolution of the non-increasing modified total energy of the proposed model. Note that the modified energy has been normalized by the initial energy. The inset figures are the slices($x = 0, y = 0, z = 0$) of the optimal design results at the indicated times $t = 0, 5, 10, 20$ and 40 , respectively.

network in three dimension space at indicated times $t = 5, 10, 20$, and 40 , respectively. It is obvious that the thin fibres have been detached from the trunk to reconfigure the transport network. Furthermore, we demonstrate the evolution of the non-increasing energy in three dimensional space in Fig. 9. We should emphasize that the modified energy has been normalized by the initial energy. The inset subfigures show the slices($x = 0, y = 0, z = 0$) of the optimal design results at the indicated times $t = 0, 5, 10, 20$ and 40 , respectively. It can be seen from Fig. 9 that the total energy reaches a steady state at $t = 20$ and keeps non-increasing, which confirms that the proposed method is stable and works well for the biological network generation in three dimensional domain.

5. Conclusion

In this paper, we established the biological transport network system based on the phase field model. The energy cost functional is revised by considering the auxin gradient property. We modified the original energy of Cai-Hu model by adding the internal chemical potential energy into the network generating system. The revised energy function improve the stability of the boundary between different phases while insignificantly affect the vector field of the conduct vector \mathbf{m} . Then we derived the complicated model with a gradient flow system by minimizing the modified energy. This phase-field based network generating model coupled

306 the Poisson type equation for pressure, the reaction-diffusion type equation for the network conductance,
307 and the Allen-Cahn type equation for phase field. We have rigorously proved the energy dissipation law
308 with continuum functionals. In order to obtain the second-order temporal accuracy, we applied the Crank-
309 Nicolson-type method for the governing system. Although we considered only semi-explicit schemes in time,
310 our algorithm is stable for the stiff issues of the hybrid system. For the spatial discretization, we discretized
311 the coupling system with the central finite difference method and treated the nonlinear terms semi-explicitly
312 to form a linear system at each time step, which can be solved by a multigrid method. The discrete energy
313 dissipation was proved rigorously which confirms that a large time step can be used with the unconditional
314 stability of the implicit solver. We applied the preconditioned conjugate gradient method with the multigrid
315 method as a preconditioner to implement a practical algorithm with only linear algebraic complexity and
316 achieve fast convergence. The discretized system for the phase-field based model was decoupled, linear,
317 and unconditional stable and the proposed algorithm was easy to implement. We note that the proposed
318 scheme can serve as a building block to design accurate and stable linear schemes for a class of gradient
319 flow problems with high degree of nonlinearity. Various numerical tests were demonstrated to validate the
320 efficiency, stability and robustness of the proposed scheme.

321 Acknowledgment

322 Y.B. Li is supported by National Natural Science Foundation of China (No. 12271430). Q. Xia is
323 supported by the Fundamental Research Funds for the Central Universities, China (No. XYZ022022005).
324 The authors are grateful to the reviewers whose valuable suggestions and comments significantly improved
325 the quality of this paper.

326 References

- 327 [1] M. Kraning, E. Chu, J. Lavaei, S. Boyd, Dynamic Network Energy Management via Proximal Message Passing, Found.
328 Trends. Opt., 1 (2014) 70–122.
- 329 [2] H. Ushijima-Mwesigwa, Z. Khan, M. Chowdhury, I. Safro, Centralities for networks with consumable resources, Netw.
330 Sci., 7 (2019) 376–401.
- 331 [3] S. Park, O. Simeone, O. Sahin, S. Shitz, Fronthaul compression for cloud radio access networks: Signal processing advances
332 inspired by network information theory, IEEE Signal Proc. Mag., 31 (2014) 69–79.
- 333 [4] J. Garnier, G. Billen, E. Hannon, S. Fonbonne, Y. Videnina, M. Soulie, Modelling the transfer and retention of nutrients
334 in the drainage network of the Danube River, Estuar. Coast. Shelf S., 54 (2002) 285–308.
- 335 [5] Q. Xia, G. Sun, Q. Yu, J. Kim, Y. Li, Thermal-fluid topology optimization with unconditional energy stability and
336 second-order accuracy via phase-field model, Commun. Nonlinear Sci. Numer. Simul., 116 (2023) 106782.
- 337 [6] Y. Lu, D. Hu, Optimisation of biological transport networks, E. Asian J. Appl. Math., 12 (2022) 72–95.
- 338 [7] G.D. Yancopoulos, S. Davis, N.W. Gale, J.S. Rudge, S.J. Wiegand, J. Holash, Vascular-specific growth factors and blood
339 vessel formation, Nature, 407 (2000) 242–248.

- 340 [8] A. Runions, M. Fuhrer, B. Lane, P. Federl, A.G. Rolland-Lagan, P. Prusinkiewicz, Modeling and visualization of leaf
 341 venation patterns, *ACM T. Graphic.*, 24 (2005) 702–711.
- 342 [9] D.P. Bebber, J. Hynes, P.R. Darrah, L. Boddy, M.D. Fricker, Biological solutions to transport network design, *P. Roy.
 343 Soc. B-Biol. Sci.*, 274 (2007) 2307–2315.
- 344 [10] G.E. Cantarella, E. Casetta, Dynamic processes and equilibrium in transportation networks: towards a unifying theory.
 345 *Transport. Sci.*, 29 (1995) 305–329.
- 346 [11] S. Bohn, M.O. Magnasco, Structure, scaling and phase transition in the optimal transport network, *Phys. Rev. Lett.*, 98
 347 (2007) 088702.
- 348 [12] D. Hu, D. Cai, Adaptation and optimization of biological transport networks, *Phys. Rev. Lett.*, 111 (2013) 138701.
- 349 [13] H. Ronellenfitsch, E. Katifori, Global optimization, local adaptation, and the role of growth in distribution networks,
 350 *Phys. Rev. Lett.*, 117 (2016) 138301.
- 351 [14] E. Katifori, G.J. Szöllosi, M.O. Magnasco, Damage and fluctuations induce loops in optimal transport networks, *Phys.
 352 Rev. Lett.*, 104 (2010) 048704.
- 353 [15] F. Corson, Fluctuations and redundancy in optimal transport networks, *Phys. Rev. Lett.*, 104 (2010) 048703.
- 354 [16] A. Barabasi, R. Albert, Emergence of scaling in random networks, *Science*, 286 (1999) 509–512.
- 355 [17] A. Eichmann, F. Le Noble, M. Autiero, P. Carmellet, Guidance of vascular and neural network formation, *Curr. Opin.
 356 Neurobiol.*, 15 (2005) 108–115.
- 357 [18] J. Haskovec, L. Kreusser, P. Markowich, Rigorous continuum limit for the discrete network formation problem, *Commun.
 358 Partial Differ. Equ.*, 44 (2019) 1159–1185.
- 359 [19] R. Budzinski, B. Boaretto, T. Prado, S. Lopes, Synchronization domains in two coupled neural networks, *Commun.
 360 Nonlinear Sci. Numer. Simul.*, 75 (2019) 140–151.
- 361 [20] O. Michel, J. Biondi, Morphogenesis of neural networks, *Neural. Proc. Lett.*, 2 (1995) 9–12.
- 362 [21] N. Dengler, J. Kang, Vascular patterning and leaf shape, *Curr. Opin. Plant. Biol.*, 4 (2001) 50–56.
- 363 [22] Z. Zhang, C. Zhu, Q. Wang, J. Yuan, Discrete robustness optimization on emergency transportation network based on
 364 prospect theory, *J. Adv. Transport.*, 2019 (2019).
- 365 [23] J. Sienkiewicz, P. Fronczak, J. A. Holyst, Log-periodic oscillations due to discrete effects in complex networks, *Phys. Rev.
 366 E.*, 75 (2007) 066102.
- 367 [24] H. Du, P. Perre, I. Turner, Modeling fungal growth with fractional transport models, *Commun. Nonlinear Sci. Numer.
 368 Simul.*, 84 (2020) 105157.
- 369 [25] A. Tero, S. Takagi, T. Saigusa, K. Ito, D. Bebber, M. Fricker, K. Yumiki, R. Kobayashi, T. Nakagaki, Rules for biologically
 370 inspired adaptive network design, *Science*, 327 (2010) 439–442.
- 371 [26] D. Hu, D. Cai, An optimization principle for initiation and adaptation of biological transport networks, *Commun. Math.
 372 Sci.*, 17 (2019) 1427–1436.
- 373 [27] M. Burger, J. Haskovec, P. Markowich, H. Ranetbauer, A mesoscopic model of biological transportation network, arXiv
 374 preprint arXiv:1806.00120, 2018.
- 375 [28] G. Albi, M. Artina, M. Foransier, P. Markowich, Biological transportation networks: modeling and simulation, *Anal.
 376 Appl.*, 14 (2016) 185–206.
- 377 [29] C. D. Murray. The Physiological Principle of Minimum Work: I. The Vascular System and the Cost of Blood Volume.
 378 *Proc. Natl. Acad. Sci. USA*, 12(3):207–214, 1926.
- 379 [30] J. Haskovec, P. Markowich, B. Perthame, Mathematical Analysis of a PDE System for Biological Network Formation,
 380 *Commun. Part. Diff. Eq.*, 40 (2015) 918–956.
- 381 [31] J. Haskovec, P. Markowich, B. Perthame, M. Schlottbom, Notes on a PDE system for biological network formation,
 382 *Nonlinear Anal.*, 138 (2016) 127–155.

- 383 [32] B. Li, On the blow-up criterion and global existence of a nonlinear PDE system in biological transport networks, *Kinet.*
 384 *Relat. Mod.*, 12 (2019) 1131–1162.
- 385 [33] B. Li, X. Li, A cross-diffusive evolution system arising from biological transport network, *Commun. Nonlinear Sci. Numer.*
 386 *Simulat.*, 92 (2021) 105465.
- 387 [34] H. Ronellenfitsch, J. Dunkel, M. Wilczek, Optimal noise-canceling networks, *Phys. Rev. Lett.*, 121 (2018) 208301.
- 388 [35] D. Fang, S. Jin, P. Markowich, B. Perthame, Implicit and semi-implicit numerical schemes for the gradient flow of the
 389 formation of biological transport network, *J. Comput. Math.*, 5 (2019) 229–249.
- 390 [36] Q. Hong, J. Li, Q. Wang, Supplementary variable method for structure-preserving approximations to partial differential
 391 equations with deduced equations, *Appl. Math. Lett.*, 110 (2020) 106576.
- 392 [37] Q. Hong, J. Zhao, Q. Wang, Energy-production-rate preserving numerical approximations to network generating partial
 393 differential equations, *Comput. Math. with Appl.*, 84 (2021) 148–165.
- 394 [38] E. Facca, F. Cardin, M. Putti, Branching structure emerging from a continuous optimal transport model, *J. Comput.*
 395 *Phys.*, 447 (2021) 110700.
- 396 [39] W. Hu, D. Wang, X.P. Wang, An efficient iterative method for the formulation of flow networks, *Commun. Comput. Phys.*,
 397 31 (2022) 1317–1340.
- 398 [40] Q. Yu, Q. Xia, Y. Li, A phase field-based systematic multiscale topology optimization method for porous structures design,
 399 *J. Comput. Phys.*, 466 (2022) 111383.
- 400 [41] Y. Li, K. Wang, Q. Yu, Q. Xia, J. Kim, Unconditionally energy stable schemes for fluid-based topology optimization,
 401 *Commun. Nonlinear Sci. Numer. Simulat.*, 111 (2022) 106433.
- 402 [42] T. Xue, Z. Gan, S. Liao, J. Cao, Physics-embedded graph network for accelerating phase-field simulation of microstructure
 403 evolution in additive manufacturing, *npj Comput. Mater.*, 8 (2022) 201.
- 404 [43] Y. Li, Q. Xia, S. Yoon, C. Lee, B. Lu, J. Kim, Simple and efficient volume merging method for triply periodic minimal
 405 structures, *Comput. Phys. Commun.*, 264 (2021) 107956.
- 406 [44] Z. Huang, G. Lin, A. M. Ardekani, A consistent and conservative volume distribution algorithm and its applications to
 407 multiphase flows using PhaseField models, *Int. J. Multiphase Flow*, 142 (2021) 103727.
- 408 [45] Q. Xia, J. Kim, Y. Li, Modeling and simulation of multi-component immiscible flows based on a modified Cahn-Hilliard
 409 equation, *Eur. J. Mech. B-fluid.*, 95 (2022) 194–204.
- 410 [46] Y. Li, Q. Xia, C. Lee, S. Kim, J. Kim, A robust and efficient fingerprint image restoration method based on a phase-field
 411 model, 123 (2022) 108405.
- 412 [47] J. Wang, Q. Xia, B. Xia, Fast Image restoration method based on the L_0 , L_1 , and L_2 gradient minimization, *Mathematics*,
 413 10 (2022) 3107.
- 414 [48] L. Onsager, S. Machlup, Fluctuations and irreversible processes, *Phys. Rev.*, 91 (1953) 1505–1512.
- 415 [49] Q. Xia, Q. Yu, Y. Li, A second-order accurate, unconditionally energy stable numerical scheme for binary fluid flows on
 416 arbitrarily curved surfaces, *Comput. Methods Appl. Mech. Engrg.*, 384 (2021) 113987.
- 417 [50] P. Dimitrov, S.W. Zucker, A constant production hypothesis guides leaf venation patterning, *P. Natl. Acad. Sci. USA*,
 418 103 (2006) 9363–9368.
- 419 [51] K. Ljung, R.P. Bhalerao, G. Sandberg, Sites and homeostatic control of auxin biosynthesis in arabidopsis during vegetative
 420 growth, *Plant. J.*, 28 (2001) 465–474.
- 421 [52] Trottenberg U, Oosterlee C, Schüller A. Multigrid. USA: Academic Press; 2001.
- 422 [53] J. Kim, H. Bae, An unconditionally gradient stable adaptive mesh refinement for the Cahn-Hilliard equation, *J. Korean*
 423 *Phys. Soc.*, 53 (2008) 672–679.
- 424 [54] Q. Xia, J. Yang, Y. Li, On the conservative phase-field method with the N-component incompressible flows, *Phys. Fluids.*,
 425 35 (2023) 012120.

- 426 [55] S. Esedoḡ, F. Otto, Threshold dynamics for networks with arbitrary surface tensions, Commun. Pur. Appl. Math., 68
427 2015 808-864.
- 428 [56] Y. Li, K. Qin, Q. Xia, J. Kim, A second-order unconditionally stable method for the anisotropic dendritic crystal growth
429 model with an orientation-field, Appl. Numer. Math., 184 (2023) 512-526.
- 430 [57] J. Zhang, X. Yang, A fully decoupled, linear and unconditionally energy stable numerical scheme for a melt-convective
431 phase-field dendritic solidification model, Comput. Methods Appl. Mech. Engrg., 363 (2020) 112779.
- 432 [58] Y. Li , J. Yang, Consistency-enhanced SAV BDF2 time-marching method with relaxation for the incompressible
433 Cahn–Hilliard–Navier–Stokes binary fluid model, Commun. Nonlinear Sci. Numer. Simulat., 118 (2023) 107055.
- 434 [59] A. Keen, A. Fenna, J. McConnell, M. Sherratt, P. Gardner, H. Shiels, The dynamic nature of hypertrophic and fibrotic
435 remodeling of the fish ventricle, Front. Physiol., 6 (2016) 427.